ZIRCONIUM PHYTATE-BASED PROTON CONDUCTORS FOR HIGH-TEMPERATURE FUEL CELL APPLICATIONS

by

Wessam Ahmed Mohamed Nimir

A Thesis presented to the faculty of the
American University of Sharjah
College of Engineering
In Partial Fulfilment
of the Requirements
for the Degree of

Master of Science in
Chemical Engineering

Sharjah, United Arab Emirates

April 2023

Declaration of Authorship

I declare that this thesis is my own work and, to the best of my knowledge and belief, it does not contain material published or written by a third party, except where permission has been obtained and/or appropriately cited through full and accurate referencing.

Signed: Wessam Ahmed Mohamed Nimir

Date:30/04/2023

Approvals

We, the undersigned, approve the Masters Thesis written by: Wessam Ahmed Nimir

Thesis Title: Zirconium phytate-based proton conductors for high-temperature fuel cell applications

Date of Defense: 27-April-2023

Name, Title and Affiliation	**Signature**
Dr. Amani Al-Othman Associate Professor Department of Chemical and Biological Engineering Thesis Advisor	
Dr. Muhammad Tawalbeh Associate Professor Department of Sustainable & Renewable Energy Engineering University of Sharjah Thesis Co-advisor	
Dr. Yassir Makkawi Professor Department of Chemical and Biological Engineering Thesis Examiner (Internal)	
Dr. Oussama El-Kadri Associate Professor Department of Chemistry University Name: AUS Thesis Examiner (External)	

Accepted by:

Dr. Fadi Al-Oul
Dean
College/School of Engineering

Dr. Mohamed El-Tarhuni
Vice Provost for Research and Graduate Studies Office of Research and Graduate Studies

Acknowledgments

In essence, all praises to Almighty Allah for giving me the strength and ability to complete this work and for all his blessings in every step of my life.

Secondly, I would like to thank my advisors Dr. Amani Al-Othman and Dr. Muhammad Tawalbeh for providing knowledge, guidance, support, and motivation throughout my research stages. I'm deeply beholden for their great assistance, worthy discussion, and suggestions.

Moreover, I would like to thank the professors of the Chemical Engineering department who taught me master-level courses with exceptional teaching methods and skills. I really appreciate their dignified advice and motivation.

Also, I deeply thank the American University of Sharjah (AUS), Dr. Amani Al-Othman and Dr. Sameer Al-Asheh for providing me with Research Assistantship (GRA) and Teaching Assistantship (GTA) and for their continuous help during my graduate studies.

Finally, I would like to thank my beloved parents and my siblings for their unwavering love, support, and guidance throughout each step of my life. Last but not least, I would like to thank my friends at the American University of Sharjah for their continuous support and encouragement throughout this research.

Dedication

To my beloved parents, family, & friends…

Abstract

Hydrogen fuel cells are regarded among clean power sources. They yield almost zero emissions with water being the only product. A functional membrane is the heart of the proton exchange membrane (PEM) fuel cell. This thesis describes the development of novel composite membranes for high-temperature PEM fuel cells (HT-PEMFCs) in particular. PEM fuel cells usually operate around 80°C. HT-PEMFCs operating above water's boiling point are preferred due to their improved kinetics, heat recovery, superior water management, and enhanced tolerance to hydrogen fuel impurities. Nafion, the current conventional membrane in PEMFCs, cannot be used above 100°C, as its proton conductivity decreases dramatically. In this thesis, high-temperature and Nafion-free membranes are reported. These membranes are based on zirconium phytate (ZrPA), Silicotungstic acid (STA), and ionic liquids (ILs). Porous polytetrafluoroethylene (PTFE) polymer was used as a support. Various mass percentages of STA, and ILs were utilized and investigated. The membranes were characterized by electrochemical spectroscopy (EIS) and showed promising proton conductivity upon the addition of ILs. The unmodified ZrPA membrane had a proton conductivity of 6.65×10^{-4} S/cm. The inclusion of STA resulted in a ten-fold increase, raising it to 2.23×10^{-3} S/cm. This work investigated the effect of adding a plasticizer agent, polyethylene glycol (PEG). Further modification with PEG raised the proton conductivity to 3.81×10^{-2} S/cm. The maximum proton conductivity (0.1 S/cm), similar to Nafion's conductivity, was obtained with 5.86 wt% of the IL ([HMIM][$C_4N_3^-$]). A high-temperature test up to 150°C showed a decrease in conductivity by two orders of magnitude (10^{-3} S/cm) but, promising conductivity. Water uptake analysis revealed that the modified ZrPA/STA/PEG/ILs membranes could hold more than 60 wt% of water. The modified membranes were further characterized by TGA, SEM, EDX, and XRD. The TGA results showed a decrease of 34 wt% at 600°C. FTIR and XRD analysis indicated a change in their crystalline and revealed substantial changes in particle diameter and morphology. The previous results showed that the synthesized membranes in this thesis are of great potential for HT-PEMFC applications.

Keywords: HT-membranes, fuel cells, Zirconium phytate (ZrPA), Silicotungistic acid (STA), Polyethylene glycol (PEG), Ionic Liquids (ILs).

Table of Contents

List of Figures

List of Tables

List of Abbreviations

AFC	Alkali Fuel Cell
BPSH	Di sulfonated Poly (arylene ether sulfone)
CESH	Controlled environment sample holder
CsPOMo	Cesium Salt of Heteropoly acids
DMFC	Direct Methanol Fuel Cell
EIS	Electrochemical impedance spectroscopy
[EMIM] [BTI]	1-ethyl-3 methylimidazolium-bis (trifluoro methane sulfonyl) imide ionic liquid
FC	Fuel Cell
GDL	Gas Diffusion Layer
[HMIM][$C_4N_3^-$]	1-hexyl-3-methyl imidazolium tricyanomethanide
HT-PEMFCs	High-temperature PEMFCs
HOR	Hydrogen Oxidation Reaction
HPAs	Heteropolyacids
HPW/PTA	Phosphotungistic acid
ILs	Ionic liquids
ITS	Intermediate temperature system
LT-PEMFCs	Low-temperature PEMFCs
MEA	Membrane exchange assembly
MCFC	Molten Carbonate Fuel Cell
MCM-41	Mesoporous Silica nanocomposites
ORR	Oxygen Reduction Reaction
PA	Phosphoric Acid

PAFC	Phosphoric Acid Fuel Cell
PBI	Polybenzimidazole
PEG	Polyethylene glycol
PEMFC	Proton Exchange Membrane Fuel Cells
PES-PVP	Polyether sulfone-Polyvinylpyrrolidone
POMs	Polyoxometalates
Pt	Platinum
PTFE	Polytetrafluoroethylene
PWA	Phosphotungstic Acid
QDPSU	Quaternary Diazabicyclo-Octane Polysulfone
RH	Relative Humidity
Semi-IPN	Semi-interpenetrating polymer networks
SiWA/STA	Silicotungstic Acid
SOFC	Solid oxide Fuel Cell
SPAES	Sulfonated poly (arylene ether sulfone)
SPEEK	Sulfonated poly ether ether ketone
SPEI	Sulfonate polyetherimide
TSA	Tungstosilicic acid
ZrP	Zirconium phosphate
ZrPA	Zirconium phytate
ZrNT	Zirconium oxide nanotubes

Chapter 1. Introduction

1.1. Overview

In history, humans have utilized a wide range of energy sources, including coal, wind, hydro-energy, geothermal, solar, and fossil fuels. However, fossil fuels have been primarily used [1]. The reliance on fossil fuels has led to a depletion that results in serious economic instability in several countries, along with fluctuations in oil prices [2]. In addition, they have detrimental effect on the environment and ecosystem due to excessive pollutant emissions [3][4]. Carbon dioxide, which is one of these emissions is considered the primary cause of global warming [5][6]. Consequently, studies have been focused on renewable energy sources [7]. Fuel cells are electrochemical devices that convert chemical energy into electrical energy [8]. They have been developed for different applications, and they can be categorized by fuel type and convertor, oxidizing agents, generators, electrolytes, and operating temperatures [9]. When hydrogen is the fuel, fuel cells are regarded among the clean power sources where the only product is water.

The first fuel cell was firstly described in 1839 by Sir William Robert Grove [10]. He immersed platinum electrodes in sulfuric acid and introduced hydrogen/oxygen gas as the fuel [11]. Ludwig Mond (1839–1909) and Charles Langer used coal as fuel and introduced the fuel cell term to describe 20 Am^{-2} at 0.73 V [12]. In 1932, British engineer Francis Bacon modified Langer's and Mond's cells to create the first alkaline fuel cell, which was used later in Apollo space craft. William W. Jacques [13] invented the first practical fuel cell in 1896, while Walther Nernst was the first to employ zirconium as a solid electrolyte in 1900. After that in 1950, the first polymer electrolyte membrane fuel cell which was designed by Willard Thomas Grubb and Leonard Niedrach was used by NASA in the Gemini space program. They were using sulfonated polystyrene as their polymer, but it was replaced by Nafion in 1966 [8]. In 1961 G.V. Elmore and H.A. Tanner synthesized a fuel cell that could operate with air directly without the need for pure oxygen and it could work for 6 months without any deterioration at 90 mA/cm^2 and 0.25 V [13]. Its electrolyte was made of a mixture of phosphoric acid and silicon dust based on a Teflon. After that PEMFCs started to get huge interest, due to their high efficiency and zero to low emissions to the atmosphere when hydrogen is used as fuel.

The proton exchange membrane (PEM) is considered as the core component of the fuel cell, as it facilitates the movement of protons or hydrogen ions from the anode to the cathode to allow the completion of redox reaction [14]. Among the various polymers that have been used in fuel cells, Nafion is the commercially available proton-conducting membrane, and it's known as the standard polymer that any new composite membrane is compared to it. It was created by DuPont in the late 1960s. It has high proton conductivity (0.1 S/cm), due to its sulfonated Perfluorinated polyethylene backbone structure. In addition, it has high thermal and mechanical stability at temperatures below 90℃ [15]. However, at elevated temperatures above 90℃, it shows a dramatic reduction in its proton conductivity, due to the dehydration of ionic clusters of its structure, which results in a considerable reduction in PEMFC performance. Another issue is Nafion's high cost, which is preventing widespread manufacture and commercialization [16].

High- temperature operation is preferred in fuel cells for several reasons. It improves the reaction kinetics of fuel cells, enhances water management, it allows the recovery of unused heat and increases the resistance to catalyst poisoning, thus, allowing the usage of various types of fuels [17][18]. As a result, there is an outstanding effort for developing HT-PEMFCs. Many HT-PEM has been synthesized in the literature. They were developed by two strategies. One of them depends on polymers that work at low water content conditions with their proton conductivity not being affected. While the other is concerned with the anhydrous conditions, where the proton movement is not aided by water [19]. In both methods, various types of fillers and plasticizers are utilized [14].

In this thesis, a new composite Nafion-free membranes are synthesized. They are composed of zirconium phytate (ZrPA) with Silicotungstic acid and other additives such as polyethylene glycol, and Ionic Liquids. These membranes have been investigated for their proton conductivity, morphology, water uptake, and theirs chemical and mechanical stability at high temperatures. The objective of this work is to develop a high proton conductive membrane that could handle the elevated temperatures (>80 °C to 150°C) and can increase the performance of the polymer electrolyte membrane fuel cells (PEMFCs) in sustainable power supply for different applications.

1.2. Thesis Objective

The purpose of this work is the synthesis of Nafion-free solid proton conductors based on zirconium phytate (ZrPA), Silicotungstic acid, PEG and ionic liquids for high-temperature PEM fuel cell applications. This combination of materials is introduced for the first time in the PEMFCs, due to the high chemical and thermal stability of each material as well as their high protonic conductivity which can lead to an increase in the PEMFC's performance in sustainable power supply.

The main objectives of this work are:

1. Synthesize new proton conducting membranes based on zirconium phytate and silicotungstic acid.
2. Study the effect of the addition of poly-ethylene glycol, and two imidazolium based ionic liquids (1-Hexyl-3- methylimidazolium tricyanomethanide) and (1-Ethyl-3-methyl imidazolium biscteifluoromethyl sulfonyl imide) on the proton conductivity and find the best conductive composite membrane of zirconium phytate and silicotungstic acid.
3. Conduct a full characterization for the membranes to evaluate their proton conductivity, chemical structure and water uptake properties using electrochemical impedance spectroscopy (EIS) coupled with the intermediate temperature system (ITS), Scanning electron microscopy (SEM), Fourier transform infrared spectroscopy (FTIR), X-ray diffraction (XRD), Energy dispersive X-ray (EDX) and thermogravimetric analysis (TGA).

1.3. Research Contribution

The contributions of this research work can be summarized as follows:

- The research proposes novel-composite membranes for PEMFCs, for high temperature operations. These membranes can overcome the drawbacks of the current state of art, the Nafion at elevated temperatures. They show a significant stability in the proton conductivity at temperatures above 100°C, while maintaining the mechanical and chemical stability.
- The synthesis of potentially lower cost high temperature membrane compared to Nafion's cost.

1.4. Thesis Organization

This thesis is divided into seven chapters. The first chapter gives the table contents of the thesis as well as the list of figures and tables. The second chapter gives an introduction and an overview of the project and the thesis objective and contribution. The third chapter includes an extensive literature review of the PEM fuel cells, the hydrogen role in fuel cells, and the advantages of high temperature operations. In additions, it gives detailed information about the proposed materials, zirconium phytate, silicotungstic acid, PEG, and ILs. The fourth chapter discusses the materials and the methodology in details. The results of the membrane's proton conductivity are discussed in chapter five. Followed by chapter six, which presents the analysis and the discussion of the membrane's morphology, water uptake, and proton conductivity at elevated temperatures. Finally, chapter seven concludes the work and the future recommendations.

Chapter 2. Background and Literature Review

Chapter two represents an overview of the polymer electrolyte membrane fuel cells (PEMFCs), and the standard employed membrane (Nafion). Followed by the advantages of high temperature operations which range from the electrochemical reaction kinetics, carbon monoxide tolerance to the water and heat management. Finally, it addresses the materials that were used in the membrane's synthesis and their effect on the membrane's advancement.

2.1. Overview of PEM Fuel Cells

Fuel cells are regarded as an environmentally friendly technology, as they provide a range of environmental benefits, such as reducing harmful levels of local pollutants, in addition to providing economic benefits due to their high efficiency. In a fuel cell system, all operations are controlled by the diffusion of reactants and products, which emits almost no pollutants and greenhouse gases [10]. Hence, fuel cells can be used in a wide range of applications, including transportation, stationary appliances, and portable electronic devices, such as laptop computers, video cameras, and consumer electronics [21]. Fuel cells are classified according to their electrolyte material into six types: Polymer electrolyte membrane fuel cells (PEMFC), Direct methanol fuel cells (DMFC), Alkaline fuel cells (AFC), Phosphoric acid fuel cells (PAFC), Molten carbonate fuel cells (MCFC), and Solid oxide fuel cells (SOFC). Among all of them, PEMFCs are attracting huge attention. In reference to their compact size, relatively simple maintenance, low-temperature operation between 60 and 100°C, fast start-up and high power density [22][23][24]. Moreover, they have longer lifetime due to their high durability and the robustness of the electrolyte.

PEMFCs configuration design is regarded much simpler compared to the other types of fuel cells. They are primarily composed of bipolar plates, an anode (negative electrode), a cathode (positive electrode), and an ion-conducting material (electrolyte) which is sandwiched between the two electrodes [25]. The MEA membrane is the fundamental component of a proton exchange fuel cell. It is mainly composed of two layers: The membrane and a dispersed catalyst layer with a permeable Gas-Diffusion Layer (GDL) [26]. The catalyst layer is usually made of platinum (pt) due to its high performance compared to the other types of catalysts. However, its high cost is regarded

as one of the primary reasons that limit the PEM fuel cell's commercialization [27]. Figure 1 represents a schematic diagram of a PEMFC.

The fuel such as hydrogen is delivered continuously to the fuel cell through the anode. Then by an electrochemical reaction, the inserted fuel is electro-oxidized on the catalyst layer into its protons and electrons. Electrons are transferred through an external circuit to produce electricity, as the membrane is made of a proton-conductive substance. On the other hand, proton ions transfer through the membrane and combine with the reduced oxygen ions on the cathode forming water primarily as a by-product [28]. The by-product depends on the type of fluid, as CO_2 could be produced as a by-product if hydrocarbon fuel is utilized [25].

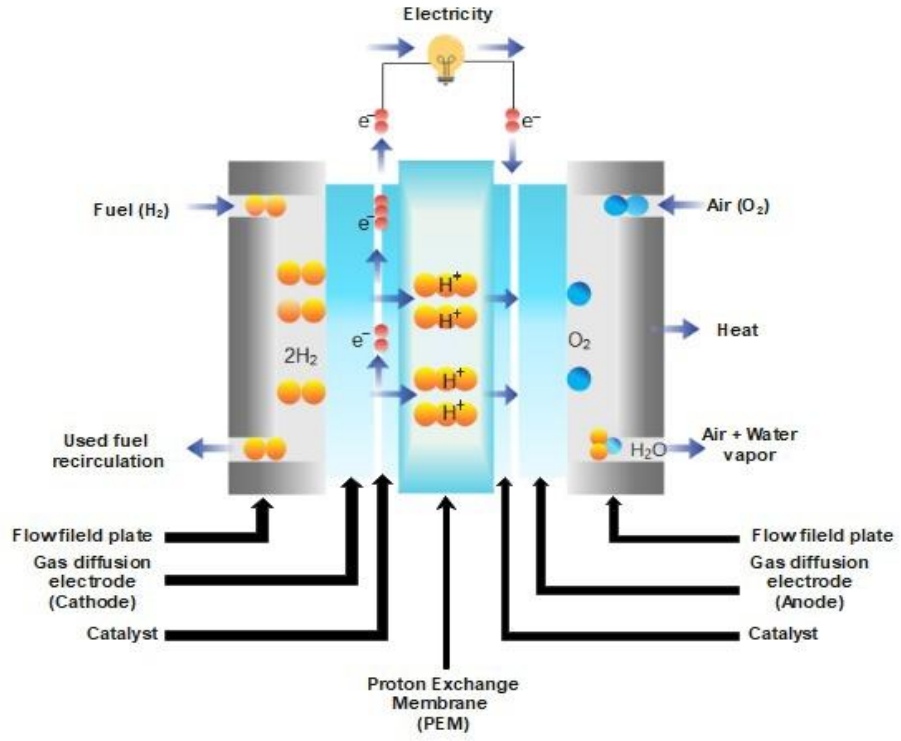

Figure 1: proton exchange membrane fuel cell diagram [29].

The two main reactions that occur on the anode and the cathode are explained as follows [30]:

At the anode the hydrogen is electro-oxidized producing hydrogen protons (H^+) and electrons (e^-):

$$H_2 \rightarrow 2H^+ + 2e^- \quad (1)$$

At the cathode the hydrogen ions (H^+) are combined with the oxygen and electrons forming water as follows:

$$½O2 + 2H^+ + 2e^- \rightarrow H2O \quad (2)$$

The overall reaction can be written as:

$$H2 + ½\,O2 \rightarrow H2O \quad (3)$$

The efficiency and effectiveness of PEMFCs are extensively dependent on the membrane properties and characteristics. These features range from chemical, mechanical, and thermal stability to high proton conductivity and low cost. As a result, Nafion is the most commonly used membrane as it possesses most of these features, except its diminishing ionic conductivity at temperatures above 80°C, fuel crossover, and expensive cost. Consequently, research put much effort over the years into improving the quality of the membranes to meet applications requirements.

2.2. Hydrogen Fuel for Fuel Cells

The extensive reliance on fossil fuels has hastened environmental degradation by causing the formation of global warming gases such as carbon, nitrogen, sulphur, and other harmful oxides [31]. Hydrogen is regarded as one of the most eco-friendly fuels that can be utilized to meet future energy demands [32]. It has almost zero-emissions, which results in a lower environmental impact. It can be produced using both renewable energy sources and fossil fuels, and while the former is less efficient than the latter, it produces free-carbon hydrogen, which is considered one of the cleanest energy elements [33][34].

Hydrogen is expected to be a perfect replacement of conventional fuels due to its inherently immense energy content, low atomic mass, zero- emissions, and its availability. These merits expanded the hydrogen applications as an efficient energy source and carrier, especially in fuel cells for power generations [35][36].

2.2.1. Production and storage of hydrogen

Hydrogen is one of the most abundant elements in the universe, despite the fact that it is only found in a form of a chemical compound rather than a free element [37]. It is mostly found in water, hydrocarbons, fossil fuels, biomass and other renewable energy sources such as wind, geothermal, and solar [34].

Hydrogen can be produced by various methods depending on the type of hydrogen source. For example, hydrogen can be produced from water using one of the following methods: solar heat, electrolysis, chemical, and photochemical reactions [38]. On the other hand, it can be produced from biomass through fermentation process under low light intensity and low temperatures [34]. Hydrogen is a very light substance; hence it can easily get lost in the atmosphere. This could be attributed to its low volumetric energy density. Consequently, it's storage process is very difficult. However, it is usually stored either in a liquid form or a gas form under specific conditions [39]. Figure 2 depicts the diagram of hydrogen storage methods.

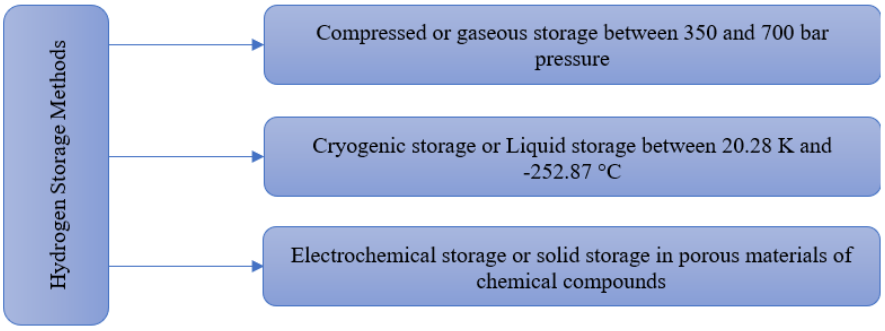

Figure 2: Some of the most common hydrogen Storage Methods [34].

2.2.2. Hydrogen in fuel cells

The periodic table shows hydrogen in both the first group and the first period. It is a relatively light gas that is present in the atmosphere but is never found there in its purest form; instead, it is typically found mixed with other elements like oxygen in the form of water. Since 2018, it has been generated from fossil fuels by partially oxidizing methane, converting steam through the gasification of coal and biomass, and electrolyzing water [40].

Hydrogen is highly suggested for use in fuel cells, due to its high energy release, which might be advantageous in high efficiency electrochemical devices. It is referred to as an energy carrier like solar energy or solar turbines as it needs to be produced from powerful energy sources [41]. When fuel cells of the electric power generation system employ hydrogen as a fuel, it undergoes oxidation on the anode, generating protons and electrons. While the protons flow through the membrane and react with the reduced oxygen and electrons on the cathode to produce water and heat, the electrons pass through the wire creating electricity [42].

2.2.3. Hydrogen economy

There are three major challenges that must be overcome to move from fossil fuels system to hydrogen electrochemical devices. Firstly, the cost of hydrogen production as well as its delivery. Secondly, safety consideration of hydrogen storage for various applications. Finally, the price of hydrogen fuel cells. The use of hydrogen in fuel cells is largely dependent on those three elements. Despite these challenges, hydrogen can be produced from sustainable or renewable energy sources that don't contain any fossil fuels, such as water electrolysis, and has the potential to bring renewable energy sources into the local hydrogen transport sector. This has significant advantages in terms of energy and economic security [42].

2.3. Standard Proton Exchange Membrane (Nafion)

Nafion is considered as the most utilized membrane in fuel cells. It is defined as a random copolymer comprised of perfluoro-ether side chains terminated with sulfonic acids which are distributed randomly along the semicrystalline polymer backbone (perfluoro-ethylene) [43]. Generally, this type of polymer is used as reference material for Chlor-alkali electrolysis, water electrolysis, polymer electrolyte fuel cells, etc [44][45][46]. Due to this backbone structure, it has high proton conductivity, mechanical and thermal stability at temperatures below 80℃, and low relative humidity. At high temperatures, its proton conductivity decreases dramatically, which is considered a major drawback of its performance. Furthermore, increasing the temperature negatively affects oxygen permeability due to the reduced relative humidity (RH) effect. In the oxygen reduction reaction, an appropriate electrical path is required to activate the cathode electrode. This will allow oxygen access and activate catalytic sites, as well as proton and electron-conducting sites. Since proton conductivity is very dependent on the RH, it will experience significant reductions at high temperatures, thereby lowering oxygen permeability and, consequently, reducing fuel cell performance [28][47][48]. Nevertheless, the high fabrication cost and the low tolerance to fuel impurities such as CO and S remain as major drawbacks for fuel cells. Therefore, operating at elevated temperatures can enhance polymer electrolyte performance with improved tolerance to the impurities as well as fewer humidification issues [49].

Significant research has been done on improving Nafion's proton conductivity

by fabricating new composite Nafion membranes in the presence of low relative humidity and high temperatures [50][51][52]. Ketpang et al [53] found that water-retaining zirconium oxide nanotubes (ZrNT) embedded in perfluorosulfonic acid (Nafion) membrane showed high performance when operating under low relative humidity. A significant increase was seen in proton conductivity compared to Nafion 212 at 80°C and 50% RH. Its performance was even better at 18% RH and 80°C, as it showed a 3.1 times higher maximum power density than Nafion 212. Furthermore, a Princeton University research team [51][54] investigated high-performance MEAs using Nafion composite membranes hybridized with silica, alumina, titanium dioxide, and zirconium phosphates. The results showed that cell output ranged from 0.65-0.7 V at 120°C, 0.58-0.66 V at 130°C, and 0.35-0.45 V at 140°C, respectively. All those measurements were taken under nearly entirely humid conditions at a pressure of 3 atm. Another study in 2019, showed that the addition of hygroscopic" oxides, such as Al_2O_3, TiO_2, SiO_2 and ZrO_2, to the Nafion can overcome the humidification problem of Nafion at high temperatures by improving the water retention, however, there was no significant improvement of the proton conductivity due to the incompatibility between the Nafion and the hygroscopic additives [55]. According to forementioned findings, more study should be done to increase proton conductivity at high temperatures in order to guarantee a high fuel cell performance.

2.4. Advantages of High-Temperature Operations

2.4.1. Electrical reaction kinetics

Numerous attempts have been made to enhance the performance of electrochemical fuel cells by investigating the kinetics of the cathodic O_2 reduction reaction (ORR) at high temperatures. ORR plays a critical role in determining the overall reaction rate, except when using hydrocarbon fuels, such as direct hydrocarbon fuel cells [56][57][58]. It has been observed that the ORR has lower electrochemical kinetics in low-temperature proton exchange membrane fuel cells (LT-PEMFC) than in high-temperature PEMFC (HT-PEMFC), which leads to a decrease in cell voltage due to the overpotential in the cathode [59]. When the anodes are sufficiently hydrated, the overpotential for hydrogen oxidation reaction (HOR) is lower than that for oxygen reduction reaction (ORR). As a result, the slow ORR determines the overall electrochemical kinetics of PEMFCs when operating with hydrogen fuel. However,

dehydration can pose a significant obstacle to running PEMFC above 100℃.

Tafel equation describes the performance of PEMFC in a kinetically controlled regime is given in equation 4 [18]:

$$E = E_{rev} + b\log(i_0) - b\log(i) \tag{4}$$

where,

$$b = -2.3\,\frac{RT}{\alpha nF} \tag{5}$$

Where *E is* the electrode potential, E_{rev} is the reversible potential, *b* is the Tafel slope, *I* is the current density, i_0 is the exchange current density, *n* is the number of electrons transferred in the rate-determining step, and α is the transfer coefficient. Zhang et al [18] show variations of E_{rev}, i_0, and *b* with temperature.

According to this theory, several conclusions can be drawn. Firstly, an increase in fuel cell temperature results in a decrease in the theoretical E_{rev}. This decrease can be attributed to an increase in the water partial pressure with respect to the constant relative humidity (RH). Secondly, an experiment has demonstrated that the Tafel slope of the ORR increases at low current densities as temperature rises. However, in high current density regions, the Tafel slope remains constant. Lastly, it has been observed that i_0 increases as temperature rises below 100 ℃. However, the relationship between i_0 and temperature above this point is not well understood in the literature.

2.4.2. Carbon monoxide (CO) tolerance

CO tolerance is a crucial factor that affects the efficiency of fuel cells. It refers to the ability of a fuel cell to function efficiently even in the presence of CO without causing a significant decrease in voltage (i.e., less than 10-20 mV) at the hydrogen electrode [51]. To overcome the challenges associated with the storage, transportation, and distribution of pure hydrogen in portable and field applications, hydrogen-rich reformates are used as fuel. However, these reformates often contain approximately 1% CO [60], which can lead to a considerable drop in performance at 80°C, particularly with prolonged exposure to low CO concentrations (as low as 10 ppm) [61]. Although Pt catalyst is commonly used in fuel cells, it has a high affinity for CO, which can accumulate on the catalyst's active sites and impair its performance. Therefore, enhancing CO tolerance is an essential scientific and technological objective in fuel cell

technology.

Various techniques have been employed to improve the CO tolerance of fuel cells, such as reducing the on-set potential for CO oxidation, minimizing the amount of adsorbed CO, increasing operating temperature, and purifying the fuel feed to remove CO [62]. However, most of these methods have significant limitations, such as reduced fuel cell performance and increased system complexity resulting from the use of an oxidant [18]. Recent studies have shown that the most effective way to increase CO tolerance is by operating at high temperatures. Chandan et al.[63] showed that in low-temperature conditions, a significant amount of CO is absorbed on the Pt surface, while at high temperatures (>160℃), approximately 3% of CO can be tolerated. In fuel cells with PBI membranes, Wong et al.[14] revealed that operating at higher temperatures (around 200℃) can increase CO tolerance from 10,000 ppm to 30,000 ppm. Additionally, Cheng et al.[64] approved that at 240℃, excellent CO tolerance was achieved with minimal loss in performance even at a CO content as high as 11.7%. The improved tolerance is attributed to the thermodynamics of CO and H_2 fuel adsorption on the Pt electrocatalyst, which can be explained using Langmuir isotherms in the following equations [51]:

$$CO\ (g) + Pt \rightarrow Pt - CO \tag{6}$$

$$H_2 + 2Pt \rightarrow 2Pt - H \tag{7}$$

CO and H_2 coverage fractions (θ) on the catalyst surface are given by equations (8,9):

$$\theta_{CO} = \frac{K_{CO}P_{CO}}{1 + K_{CO}P_{CO} + K_H^{1/2}P_{H_2}^{1/2}} \tag{8}$$

$$\theta_H = \frac{K_H^{1/2}P_{H_2}^{1/2}}{1 + K_{CO}P_{CO} + K_H^{1/2}P_{H_2}^{1/2}} \tag{9}$$

Where P_{CO} and P_{H2} represent the partial pressures of CO and H_2 in the gas phase, respectively, and K_{CO} and K_H represent the adsorption equilibrium constants. Since, the process of hydrogen adsorption necessitates the utilization of two adsorption sites only, this will result in lower exothermicity compared to CO adsorption. As temperature increases, the coverage of H_2 on the catalyst surface increases, while the coverage of CO decreases. According to Figure 3, decreasing CO coverage on the

catalyst surface enhances fuel cell performance in the presence of small amounts of CO at elevated temperatures [42].

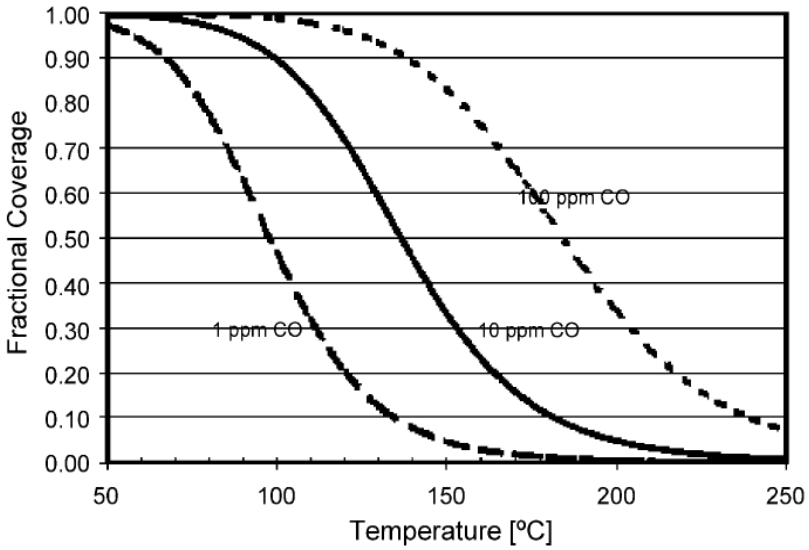

Figure 3: The coverage of CO on platinum as a function of temperature and CO concentration, H_2 partial pressure is 0.5 bar [51].

2.4.3. Water and heat management

Water management is considered a significant factor in fuel cell performance due to the high dependency of the proton ions movement on the water content. At low-temperature operation, flooding can occur due to the increase in water amount in cathode as the process temperature is below 100°C, in addition, the presence of liquid as well as vapor water causes significant water management challenges [59]. On the other hand, high-temperature operation will lead to a decrease in the proton conductivity to the dehydration [18]. Hence, to understand how to manage the flow of water inside the PEM cell, it is necessary to introduce the concept of water transport. Water production at the cathode results in a water gradient between the membranes, which causes back diffusion of water from the cathode to the anode. Additionally, a pressure difference may cause water to flow from the cathode to the anode. This phenomenon is known as electro-osmotic drag. It has been discovered that fuel cell performance is impacted by both diffusions of gas and electro-osmotic drag. Ren et al. [65] report that the fast evaporation of absorbed water decreases hydrogen bonding between water molecules as the temperature increases. As mentioned in the Grotthuss mechanism, consideration of polymetric materials in high-temperature fuel cells

applications is crucial because they can retain water, particularly bond water.

Around 50% of produced energy is dissipated as heat, due to the irreversibility of the cathodic reaction, Ohmic resistance, and mass transport overpotentials [66]. The removal of this heat is necessary to ensure the durability of the fuel cell, as it prevents dehydration, shrinkage, and cracking of the membranes as well as electrodes. The only problem that is associated with the removal of heat is the use of an existing cooling radiator, which is considered insufficient, in addition to its high cost [63]. High temperatures (above 100℃) facilitate the heat rejection from a fuel cell since they have a large temperature gradient with the surrounding environment. Consequently, this might result in a simpler cooling system. In other words, increasing the temperature of a PEMFC increases the weight and mass-specific energy densities along with its overall efficiency. Moreover, the high-temperature waste could be recovered as a stream, which can be used in many applications, such as steam reforming. In a fuel cell stack, for example, the produced steam at temperatures exceeding 200℃ can be utilized for direct heating. Consequently, optimum fuel cell efficiency is enhanced at high operating temperatures [18]. Finally, it is important to simplify water and heat management to create simpler flow designs, which might lower the overall cost of stack operation.

2.4.4. Temperature effect on oxygen diffusion

As mentioned previously, elevated temperatures lead to simplified water management due to the presence of only one phase (gaseous). In the absence of liquid to interfere with the electrochemical reactions, the reactant and product gases should diffuse faster [18]. Thus, the diffusion coefficient of oxygen through water vapor is higher than that of oxygen through liquid water. In hydrated Nafion membranes, oxygen diffusion coefficient, D_{O2}, is related to temperature (T) by equation 10 [67]:

$$D_{O_2} = 3.1 \times 10^{-3} \exp\left(-\frac{2768}{T}\right) \quad (10)$$

Based on this equation, the ratio of liquid water to water vapor decreases as the operating temperature increases (for a given current density). Accordingly, oxygen diffusion will increase. HT-PEMFCs, therefore, provide improved oxygen transport via gas diffusion layers and catalyst layers, which results in improved overall cell efficiency [63].

2.5. High-Temperature approaches

According to the literature, the Nafion-based proton exchange membrane has limitations in its operating conditions and can only function optimally under certain conditions, specifically at temperatures up to 80℃ and high humidity levels [28]. If temperatures exceed this limit, the membrane's ability to conduct protons will decrease significantly, causing problems such as CO deposition on the catalyst and reduced fuel cell performance. As a result, several techniques have been developed to maintain the conductivity of high-temperature PEMFCs without losing water, especially at temperatures near or above the boiling point of water [68]. One method involves incorporating inorganic materials into perfluorinated ionomer membranes to increase conductivity, such as adding HPAs to Nafion. Research has revealed that, the incorporation of acids into the membrane can increase the proton conductivity as well as the proton density due to the strong hydrogen bond of water molecules in the inorganic material. Another method involves using solid-state proton conductors that can operate without water, unlike the first method which requires a liquid solvent. The third approach is the utilization of non-aqueous, low-volatility solvents like ionic liquids instead of water [69]. For instance, the immobilization of acids into Nafion could separate the protons in the sulfonic acid group of Nafion. This can aid in water retention properties within the membranes and ultimately improve the composite membrane's proton conductivity. Lu et al. [70] have shown that the immobilization of phosphotungstic acid into Nafion membranes has increased the proton conductivity by four times when compared to the pristine Nafion at both low and high relative humidity. Furthermore, Xu et al. [71] found that using in-situ techniques to modify Nafion with silica (Silca/Nafion) resulted in the stabilization of water distribution within the membrane structure. The combination of targeted silica particles and efficient $–SO_3H$ based proton channels resulted in a significant improvement in the high-temperature proton conductivity of the Nafion membrane, especially at low relative humidity. The Silica-Nafion membrane exhibited a proton conductivity of 0.07 S/cm at 110 °C and 60% RH. Importantly, the mechanical, oxidative, and thermal stabilities of the Silica-Nafion membrane were not compromised due to the preservation of the original Nafion structure. Ionic liquids have been used extensively in fuel cell membranes. Karimi et al. [60] explored the feasibility of using ionic liquids instead of water in fuel cell systems and compared anhydrous fuel cells with polymers doped with ionic liquids.

This research is studying the potential of using zirconium phytate, a solid proton conductor, in conjunction with silicotungstic acid as an inorganic material and modifying them with ionic liquids for use in high-temperature fuel cell applications.

2.5.1. Zirconium phytate

Zirconium phytate is a type of inorganic compounds that composed of zirconium and phytate ions. Its chemical formula is $Zr(PO_4)_2$, and it has a crystal structure that belongs to the monoclinic space group P21/c. The zirconium ions are coordinated to eight oxygen atoms, forming a distorted square antiprism, while the phytate ions act as bridging ligands between the zirconium ions. This results in a three-dimensional network structure that is stable under a wide range of conditions. To prepare zirconium phytate, zirconyl chloride and phytic acid are combined through a process known as gelation [72]. Phytic acid is a type of plant antioxidant that contains six phosphonic acid groups per molecule, which allows it to form hydrogen bonding networks that facilitate proton conduction. Additionally, phytic acid can easily bind with metal ions such as Zr^{+4} to form coordination polymers that link adjacent phytic acid molecules with the zirconium ion. Researchers have investigated various molar ratios of ZrPA and found that the most effective ratio is 3:4, as it has given proton conductivity of 0.099 S/cm at 140℃ and 100% RH, 0.042 S/cm at 50% RH, and 0.018 S/cm at 0% RH. Electron microscope studies have shown that ZrPA has a fusiform shape and a layered structure. In addition, ZrPA (3:4) has exhibited excellent thermal stability up to 250℃. Those finding made zirconium phytate as a promising proton solid conductor for HT-PEMFCs.

2.5.2. Heteropolyacids and their role in HT-PEMFCs

Heteropolyacids (HPAs) are a group of Polyoxometalates (POMs). They consist of MO_x polyhedra (usually octahedra), where M is typically W, Mo, or V, surrounded by one or more heteroatoms. Typically, they are classified under the Wells-Dawson, Keggin, and lacunary structural configurations [73]. They have been studied extensively for the last decade due to their various selectivity of properties [74]. They have shown strong acidity, good solubility in polar solvents, good thermal stability, and reversible redox behaviour. The characteristic property of HPAs is their ability to be chemically adjusted or tuned by simply changing their structure (choosing a specific heteroatom, addendum atom, or counter ion to provide the desired stability and

electrochemical behaviour). Because of their strong acidity properties and high thermal stability, they made ideal proton conductors for fuel cells [73]. Figure 4 illustrates the Wells-Dawson and Keggin structures of heteropolyacids.

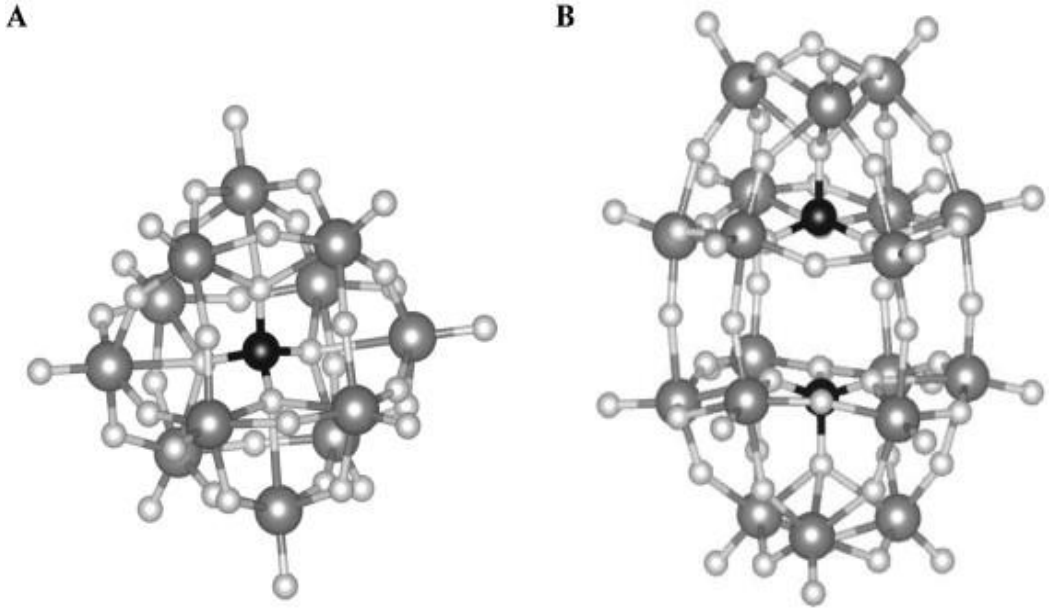

Figure 4: Ball and stick diagrams showing (A) Keggin and (B) Wells-Dawson HPA variants where phosphorus atoms are black, addenda atoms are dark grey, and oxygen atoms are light grey [73].

The addition of heteropoly acids (HPAs) can improve both the thermal and mechanical properties of polymer electrolytes while also enhancing their proton conductivity. In high-temperature proton exchange fuel cells, extensive research and development efforts are currently being conducted using polymers such as PBI, Nafion, and other polymers with HPAs. Lee et al. [75] showed that the addition of HPAs into the SiO_2 /PBI composite membrane increased the power density to 0.7 W/cm^2 at elevated temperature and low relative humidity. In 2017, study done by Nguyen et al. [76] proved that incorporation of silicotungstic acid into PBI/phosphoric acid membranes has increased the proton conductivity by one order of magnitude at 120°C. In addition, the mechanical stability of the HPAs/PBI membranes was highly increased when compared to the pure PBI membranes. Regarding the Nafion/HPAs membranes, research has found that at high temperatures (>80°C) the proton conductivity of the Nafion has enhanced due to the high thermal stability as well as the high ionic proton conductivity of heteropolyacids [73]. Lin et al.[77] created a Nafion-Silica-phosphotungstic acid (HPW) electrolyte with periodic ordering. The researchers

achieved excellent conductivity by incorporating HPA and Nafion into the mesoporous SiO_2 walls. Results were obtained for both low and high-temperature operations. At a dry condition of 200°C, the proton conductivity of the Nafion-Silica-HPA electrolyte was 0.044 S/cm. while, at a low temperature of 75 °C, the proton conductivities of the electrolyte were 0.029 S/cm and 0.09 S/cm under absolute dry (0 RH%) and fully humidified (100 RH%) conditions, respectively. Table 1 highlights the extensive research and studies that have been carried out on various polymer types, beside conventional Nafion and PBI, in conjunction with HPAs.

Table 1: The proton conductivity and Temperature and RH% of various HPA composite membranes.

Membrane type	**Temperature & % RH**	**Conductivity (S/cm) or Power density (W/cm^2)**	**Ref.**
PBI/Aquivion- SIO_2/HPA	120ºC; 40% RH	6.6×10^{-1} W/cm^2	[78]
PBI/PA	160ºC; 10% RH	4.9×10^{-2} S/cm	[79]
PBI/1.9 wt.% HPA/PA	160ºC; 10% RH	9.4×10^{-2} S/cm	[79]
PBI/3.1 wt.% HPA/PA	160ºC; 10% RH	1.27×10^{-1} S/cm	[79]
65 wt .% TSA/PBI	150ºC; anhydrous conditions	2.91×10^{-1} S/cm	[80]
50 wt.% TSA/PBI	150ºC; anhydrous conditions	2.56×10^{-1} S/cm	[80]
35 wt.% TSA/PBI	150ºC; anhydrous conditions	2.02×10^{-1} S/cm	[80]
PWA/SiO_2/PBI	100ºC; 100% RH	3×10^{-3} S/cm	[81]
PWA/SiO_2/PBI	150ºC; 100% RH	1.5×10^{-3} S/cm	[81]
50 wt.% of SiWA–SiO_2/PBI	160ºC; 100% RH	1.2×10^{-3} S/cm	[82]
50 wt.% of SiWA-SiO_2/PA/PBI	160ºC; 100% RH	2.33×10^{-3} S/cm	[83]
30wt.% PWA/ZrP/PA/PBI	200ºC; anhydrous conditions	5.8×10^{-2} S/cm	[84]
HPW/Silica/Nafion	200ºC; Dry condition	4.4×10^{-2} S/cm	[77]
PTA/Nafion	120ºC; 35% RH	1.6×10^{-2} S/cm	[85]

SiO_2/HPA/Nafion	160ºC; dry conditions	39×10^{-3} W/cm^2	[86]
SiO_2/HPA/Nafion	200ºC; dry conditions	44×10^{-3} W/cm^2	[86]
5 wt.% PWA/PES-PVP	160ºC; anhydrous conditions	1.44×10^{-1} S/cm	[87]
65 wt.% HPW/MCM-41	150ºC; anhydrous conditions	1.01×10^{-1} W/cm^2	[72]
70 wt.% HPW/MCM-41	150ºC; anhydrous conditions	1.25×10^{-1} W/cm^2	[88]
HPW-meso-silica	160ºC; anhydrous conditions	1.34×10^{-1} W/cm^2	[89]
HPA/12-phosphotungstic acid	100ºC; 80% RH	1.13×10^{-1} S/cm	[90]
PWA/Methacrylate–silica	100–150ºC; dry conditions	2.3×10^{-2} S/cm	[91]
HPA/polyether ether ketone	above 100ºC; dry conditions	10^{-1} S/cm	[92]
30 wt.% HPA/70 wt.% BPSH	130ºC; anhydrous conditions	1.5×10^{-1} S/cm	[93]
CsPOMo/QDPSU/PTFE	150ºC; dry conditions	4×10^{-2} S/cm	[94]

2.5.3. Effect of polyethylene glycol

Polyethylene glycol (PEG) is an oligomer or polymer of ethylene oxide. It is considered as one of the most important polymers or plasticizers, since it can be manufactured in a variety of molecular weights, which can be used in a wide range of applications, such as pharmaceuticals. In recent years, it has been utilized in PEMFCs. It had shown great influence on the water retention improvement due to its hydrophilic backbone. Additionally, it has exhibited high mechanical strength and thermal stability at both 70°C and 120°C, with relative humidity >50%, when compared with Nafion (117) under the same conditions [95]. PEG can also be used as a crosslinker in semi-IPN membranes to enhance both their protons conductivity and water stability at high temperatures ~100°C [96]. Thangamuthu et al.[97] fabricated crosslinked PEG/SiO2 membranes for DMFC applications. According to the results, the proton conductivity increased while the methanol permeability decreased. Also, Jodat et al.[82] had synthesized sulfonated polyetherimide (SPEI) membrane crosslinked thermally with PEG. They found that the addition of PEG increased the water uptake and the porosity of the membrane, which resulted in higher proton conductivity. Moreover, Pugalenthi et al. [99] showed that the addition of PEG to the SPEEK membrane resulted in lower

weight loss at 120℃, higher activation energy, and higher tensile stress when compared to the conventional SPEEK. As a result, PEG has been used in this research as a plasticizer and its effect on proton conductivity and thermal and mechanical stability has been investigated.

2.5.4. Effect of ionic liquids (ILs)

The incorporation of ionic liquids (ILs) in fuel cell membranes has recently gained attention in the industry due to their high proton conductivity, chemical and thermal stability, and water uptake properties [100]. There are two types of ILs: hydrophilic and hydrophobic. Hydrophilic ILs are preferred for membrane synthesis because they maintain membrane hydration, retain water, and boost proton conductivity. Ionic liquids based on imidazolium rings were the most studied due to the stability of imidazolium rings and their ability to form hydrogen bonds [101][102]. Zhang et al.[103] incorporated imidazolium-based IL (butyl-3-methylimidazolium cation with hydroxide) into a polyvinylidene fluoride/polyvinylpyrrolidone hybrid membrane and found a significant increase in conductivity from 10^{-5} S/cm without IL to 10^{-3} S/cm with IL at 80℃ and 98% relative humidity. Similarly, methylimidazolium poly (aromatic ether ketone) and fluoropolymer were used to synthesize anhydrous membranes. They exhibited a conductivity of 0.192 S/cm at 160℃ [102]. Several studies on imidazolium-based ionic liquids have shown promising results in improving proton conductivity to 10^{-3} S/cm at 150℃ for proton exchange membranes as well as enhancing anion conductivity of alkaline exchange membranes to 0.0266 S/cm at 30℃ [89][90]. In this study, 1-Hexyl-3- methylimidazolium tricyanomethanide abbreviated as [HMIM][$C_4N_3^-$] and 1-Ethyl-3-methylimidazolium bis(trifluoromethyl sulfonyl) imide [EMIM][BTI] imide have been utilized.

Chapter 3. Methodology and Experimental Work

In this chapter, several membranes of silicotungstic acid, PEG, and two imidazolium ionic liquids have been incorporated with zirconium phytate and their proton conductivity have been measured using EIS. They have been prepared using the precipitation method. Multiple characterization methods were utilized to study the chemical structure, and the proton conductivity of the fabricated materials where thermogravimetric analysis (TGA), Fourier transforminfrared spectroscopy (FTIR), scanning electron microscopy (SEM), X-ray diffraction(XRD) and electrochemical impedance spectroscopy (EIS) were all employed.

3.1. Materials

3.1.1. Zirconium oxychloride ($(ZrOCl_2)$)

The $ZrOCl_2$ used in this research is ACS 98% purity and purchased from SIGMA Aldrich.

3.1.2. Phytic acid

The $C_6H_{18}O_{24}P_6$ used in this work is 50% (w/w) in H_2O, and purchased from SIGMA Aldrich.

3.1.3. Silicotungstic acid

The Silicotungstic acid or Tungstosilicic acid hydrate $(H_4[Si(W_3O_{10})_4] \cdot xH_2O)$, has a purity ≥ 99.9% trace metal basis. It was purchased from SIGMA Aldrich.

3.1.4. Polyethylene glycol (PEG)

The $H(OCH_2CH_2)_n$ OH was purchased from SIGMA Aldrich.

3.1.5. Ionic liquids

Both ionic liquids were purchased from IoLiTec GmbH. They were used with their following purity:

1. 1-Hexyl-3-methylimidazolium tricyanomethanide [HMIM][$C_4N_3^-$] > 98%.
2. 1-Ethyl-3-methylimidazolium bis(trifluromethyle sulfonyl) imide [EMIM][BTI] > 98%.

3.2. Methodology

3.2.1. Zirconium phytate and (ZrPA) modified powder preparation

As a first step, ZrPA powder is prepared, according to the following reaction at

room temperature as can be seen in Figure 5:

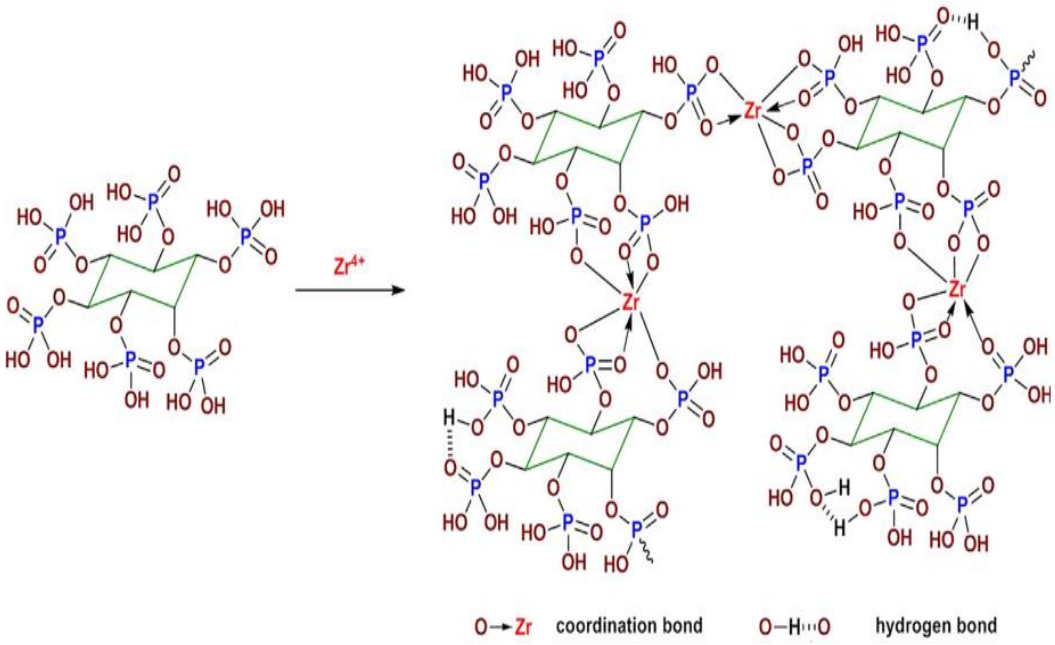

Figure 5: chemical reaction of 3:4 mole ratio of $ZrOCl_2$ to $C_6H_{18}O_{24}P_6$ [72].

The experimental procedure of preparing ZrPA powder is as follows:

1. 2.415 g of $ZrOCl_2$ was weighed and diluted in 10 ml of deionized water.
2. 9.43 g of $C_6H_{18}O_{24}P_6$ was prepared and poured to the $ZrOCl_2$ solution under the magnetic stirrer.
3. White flocculent was formed and precipitated, it was left undisturbed for 24 hours.
4. After 24 hours, the solution was dried for 2 hours at 90°C.
5. After that, the solids were grounded to powder and washed by deionized water for removal of any unreacted Phytic acid and filtered by filter paper.
6. The filtered powder then was dried again in the oven at the same temperature, and its mass was weighed.
7. Then the proton conductivity of the synthesized powder was measured using the EIS.

3.2.2. ZrPA/STA/PEG/ILs membrane preparation

Membrane synthesis process usually consists of three main steps as shown in

Figure 6:

1. The wetting step:

The $ZrOCl_2$/STA solution was prepared first for wetting the PTFE paper surface. The required amount of $ZrOCl_2$was calculated from the reaction equation. A small amount of water, around 1 ml was used to dissolve the $ZrOCl_2$ solids, to ensure that all solids were dissolved. After that, 20 ml of isopropanol was added to the solution. Various amounts of PEG and ILs were added. The mass fractions of PEG and ILs were the subject of this study. After wetting solution preparation, a piece of PTFE sheet was cut and weighed. Then it was fixed between two Teflon hoops. Then the hoops were fixed to an SCK 300P spin coater, purchased from INSTRAS as can be seen in Figure 7.

The membranes were prepared using the spin coating technique. It is a technique that is used for the fabrication of thin layers of flat surfaces. In fuel cells, it is usually used for composite membranes synthesis [106]. Among the advantages of this technique over other membrane preparation techniques is its simplicity, the ability to prepare multiple layers, and to optimize each layer separately [107]. A 0.5 ml of the alcoholic solution was introduced to the membrane via a 5 ml syringe, then the spin coater was operated, starting with 250 rpm speed for 45s, then it was raised gradually to 3250 rpm. Working at higher speeds increases the evaporation of the volatile component, which is the isopropanol in this case. After the surface is dried, another 0.5 ml was introduced, and the process was continued till the whole solution was finished.

2. The reaction step:

Wet membranes were soaked in an excess of phytic acid until they were completely covered. The sample was then placed in the fume hood for 24 hours, to ensure the reaction was completed as shown in Figure 6.

3. The drying step:

After 24 hrs the membrane was rinsed gently with deionized water, to wash any by-products that were formed during the reaction and any excess materials. Then, the membrane was placed in an oven for two hours at 90°C. After that, it was weighed and kept in zipper plastic bags for further characterization.

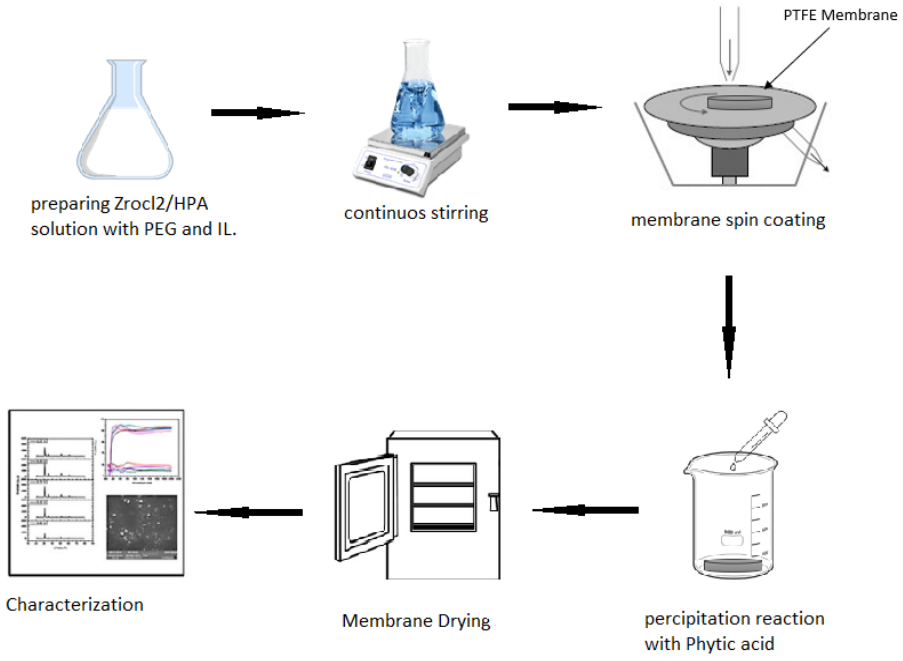

Figure 6: Schematic diagram of $ZrOCl_2$/STA composite membranes laboratory synthesis process.

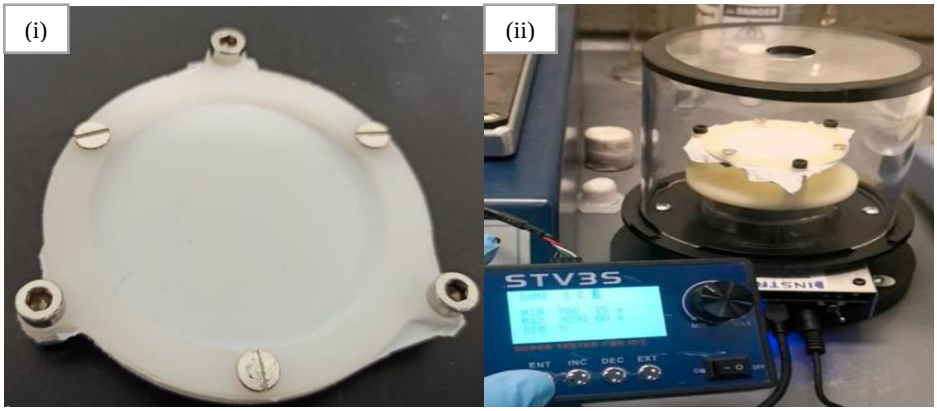

Figure 7: (i) PTFE sheet fixed between the Teflon hoops (ii) SCK 300P spin coater with the fixed Teflon hoops.

3.2.3. Characterization of synthesized ZrPA/STA/PEG/ILs membranes

The synthesized membranes were characterized using the following techniques:

3.2.3.1. Electrochemical impedance spectroscopy (EIS)

EIS is an electrochemical technique that is used for proton conductivity measurement of synthesized membranes. Bio logic SP-200 potentiostat with EC-lab software (V11.10) as can be seen in Figure 8 were used for measuring the impedance of the synthesized membranes, by applying different frequencies ranging from 100 Hz

to 7 MHz. The membrane was placed between two symmetrical stainless electrodes of a custom-made fuel cell. Then the electrodes were connected to the potentiostat via crocodile wires. An alternating potential with specific frequency was applied. The output of Z_{im}vs Z_R was reported in a Nyquist plot. Z_R represents the resistance of the membrane, the required resistance was taken by taking the intersection of the plot with the x-axis, with zero Z_{im} at the high-frequency region. The resistance value was confirmed by applying the EC-Lab software tool (Z-fit). Then this value was inserted in the following equation (11) for proton conductivity evaluation [93][86]:

$$\sigma = \frac{t}{R * A} \tag{11}$$

Where, σ represents conductivity, t represents thickness, which was measured by the digital vernier, R is the resistance, and A is the electrode cross sectional area.

Figure 8: Bio logic SP-200 potentiostat with EC-lab software (V11.10).

3.2.3.2. High-temperature test

High temperature test had been performed on the membrane with the highest proton conductivity, to test its proton conductivity at temperatures above 80°C, to check if it will maintain the same proton conductivity or not using the ITS (Intermediate Temperature System) as can be shown in Figure 9. The ITS is a compact temperature climatic chamber with a small laboratory footprint. It's used for proton conductivity measurement at high temperatures up to 150°C. It consists of two PT-1000 temperature probes, which enable the direct measurement of the actual sample temperature. The ITS is controllable via EC-Lab software using the auxiliary inputs/output of SP-200 potentiostats. The sample was prepared inside a glove box, placed in the CESH (Controlled Environment Sample Holder) and then installed in the ITS temperature

Control System for electrical characterization. Then the proton conductivity was measured using the EIS as before at different temperatures.

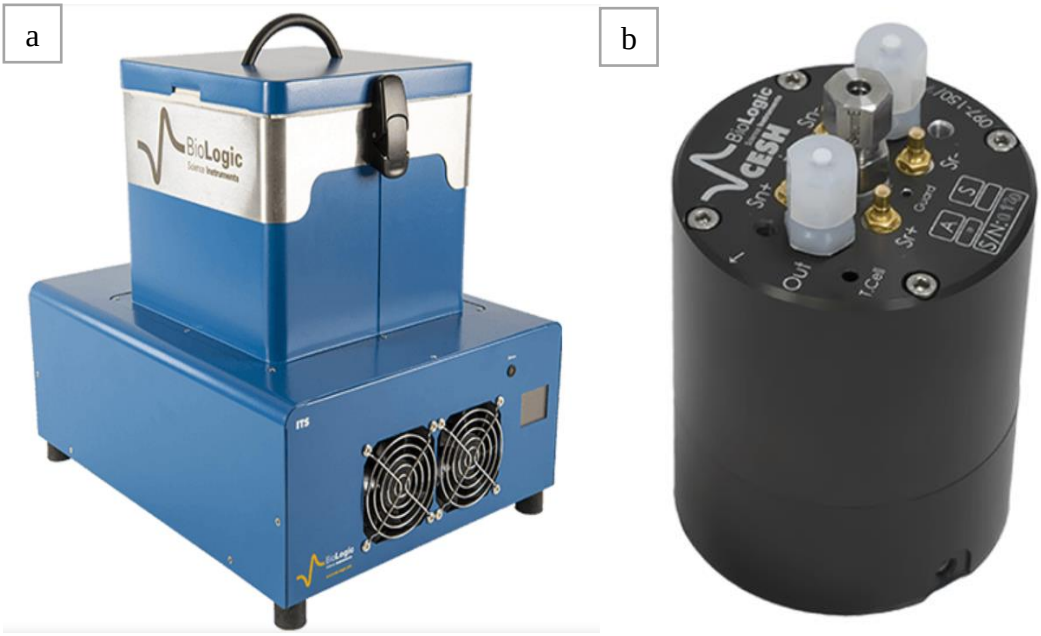

Figure 9: (a) ITS temperature climatic chamber. (b) CESH (Controlled Environment Sample Holder).

3.2.3.3. Thermogravimetric analysis (TGA)

Thermogravimetric analysis (TGA) is a thermal analysis technique that is used to determine the thermal stability of the material. It is either a function of temperature and heating rate or a function of time with the mass loss and temperature constant. The membrane samples were tested by TGA for their stability and water content loss as a function of temperature by exposing the membrane sample to heat treatment. TGA was performed on the composite membranes using PerkinElmer, model no.4000 thermogravimetric analyser. The prepared samples were subjected to a heating rate of 20°C/min over temperature range 27-900 °C. The samples weight was monitored to be between 5 to 10 mg. The process was done in the presence of Nitrogen as an inert. The TGA curves were discussed for the best conductive modified membranes.

3.2.3.4. Scanning electron microscopy (SEM)

SEM had been performed to investigate the morphology of the best membrane samples as well as their elemental composition. It was applied using Tescan VEGA XMU, LaB6 filament, Oxford Instruments X-Max 50 SSD detector. The morphology of the modified membranes was discussed and compared to the pure ZrPA.

3.2.3.5. X-Ray diffraction (XRD) and Fourier transform infrared spectroscopy (FTIR)

XRD analysis had been employed to study the crystalline structure of the membrane sample. While the FTIR had been used for identifying the molecular structure of the composite membrane as well as studying the functional group in the material. The FTIR was performed using PerkinElmer, Spectrum One FTIR Spectrometer, the wavelength range of 4000 – 400 cm^{-1}.

3.2.3.6. Water uptake analysis

The water uptake analysis was applied by measuring the membrane weight before and after hydration. The membrane sample was weighed, and its weight was recorded. After that it was immersed in deionized water for some time, and it is weight was measured again and recorded. Then the water uptake was calculated by using following equation 12:

$$water\ uptake = \frac{W_{wet} - W_{dry}}{W_{dry}} \tag{12}$$

After that, the water uptake of the synthesized membranes was analysed and compared to the Nafion's water uptake.

Chapter 4. Experimental Results & Discussion of ZrPA- based membranes

In this study, the main focus was on the modification of zirconium phytate using silicotungstic acid as a primary step. Subsequently, the addition of PEG was utilized to augment the proton conductivity. Additionally, two types of ionic liquids were investigated, and the optimal percentage composition of each component was identified to achieve the highest proton conductivity for each combination. The resulting maximum proton conductivity values for all combinations were reported.

4.1. Zirconium phytate/STA membranes

The principal objective of this research was to develop an innovative Nafion-free membrane utilizing Heteropolyacid and zirconium phytate for high-temperature polymer electrolyte membrane fuel cell (HT-PEMFC) applications. After a thorough review of the literature, silicotungstic acid was identified as the most suitable heteropolyacid due to its exceptional chemical and mechanical stability, as well as high proton conductivity at elevated temperatures [73]. In this study, silicotungstic acid was utilized to modify zirconium phytate membrane. Various STA mass percentages, ranging from 50% to 91%, were employed, and their impacts on the proton conductivity and morphology of zirconium phytate were assessed. Figure 10 illustrates the chemical structure of the utilized heteropolyacid ($H_4[SiW_{12}O_{40}]$).

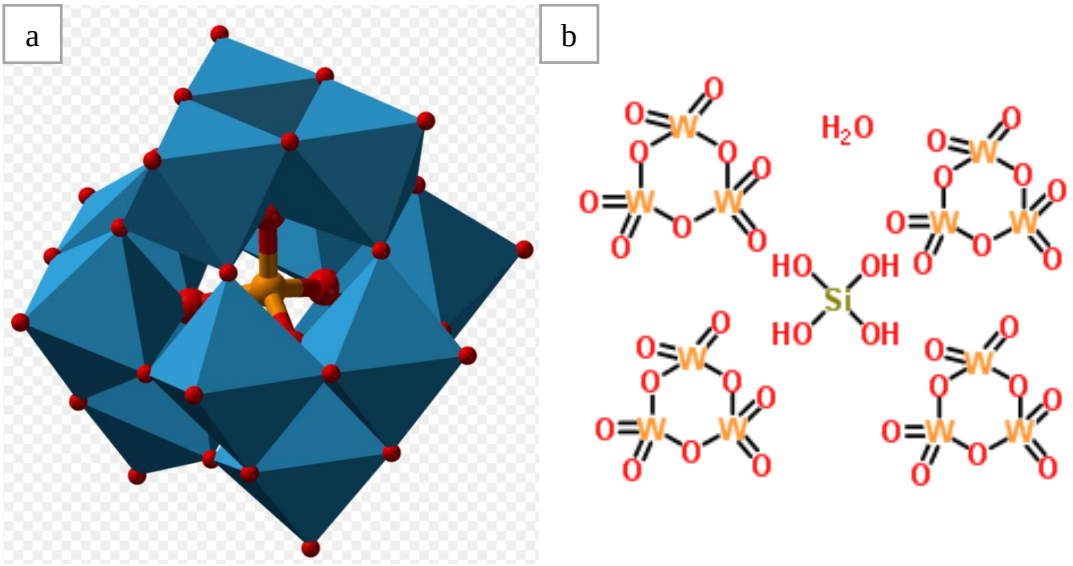

Figure 10 : (a) Silicotungstic -3D-polyhedra [109]. (b) Chemical structure of $H_4[SiW_{12}O_{40}]$ [110].

4.1.1. Proton conductivity data

The proton conductivity of zirconium phytate membrane as well as the modified zirconium phytate with silicotugistic acid were calculated at different mass ratios, and the best composite membrane was investigated with other additives such as PEG and ILs. The mass percentages of silicotungstic acid along with the specific amount of zirconium oxychloride are showed in Table 2. Six different mass percentages were immobilized into ZrPA at room temperature. According to the literature, the proton conductivity of Nafion-silicotungstic acid composite membrane was found to be $9.5 \times 10^{-2} Scm^{-1}$ at room temperature and high relative humidity [73]. Overall, silicotungstic acid membranes had the highest proton conductivity among all other types of heteropolyacids [69].

Table 2: Proton Conductivity of ZrPA/STA at different mass percentages of STA (in this work)

Zirconium phytate/Silicotungstic acid	**Mass Percentage (%) of $H_4[SiW_{12}O_{40}]$**	**Proton Conductivity (S/cm)**
ZrPA (pure)	-	6.65×10^{-4}
ZrPA/STA	50%	2.66×10^{-4}
ZrPA/ STA	67%	1.31×10^{-3}
ZrPA/ STA	75%	2.23×10^{-3}
ZrPA/ STA	86%	1.31×10^{-3}
ZrPA/ STA	89%	5.36×10^{-4}
ZrPA/ STA	91%	2.22×10^{-4}

The proton conductivity of the ZrPA/STA membranes had been investigated using electrochemical impedance spectroscopy (EIS) at high frequency region of the Nyquist plot. Figure 11 and Figure 12 show the resistance data at the high frequency region for pure ZrPA and the best ZrPA/STA respectively.

Furthermore, the resistance associated with the transport of protons across the membranes was estimated by extrapolating the Electrochemical Impedance Spectroscopy (EIS) plots to identify their intercept with the x-axis at high frequency

region. EIS plots have been categorized based on their shapes and underlying mechanisms, such as semicircles representing controlled kinetic reactions, and straight lines indicating diffusional mechanisms, which are also known as the Warburg line. Following the EIS analysis, the obtained resistance value for a given material can be plugged into Equation (11) to calculate its proton conductivity.

Results showed that, the resistance has dropped dramatically from 139.09 ohm for pure zirconium phytate membrane to 17.95 ohms for ZrPA/STA composite membrane, which results in increasing the conductivity by 3 times.

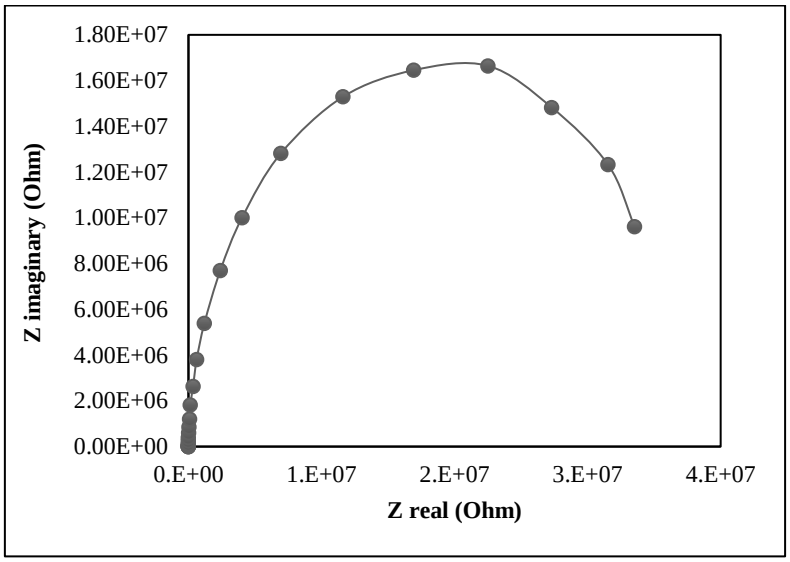

Figure 11: Nyquist plot for pure ZrPA membrane with $Z_{real} = 139.09$ Ohms

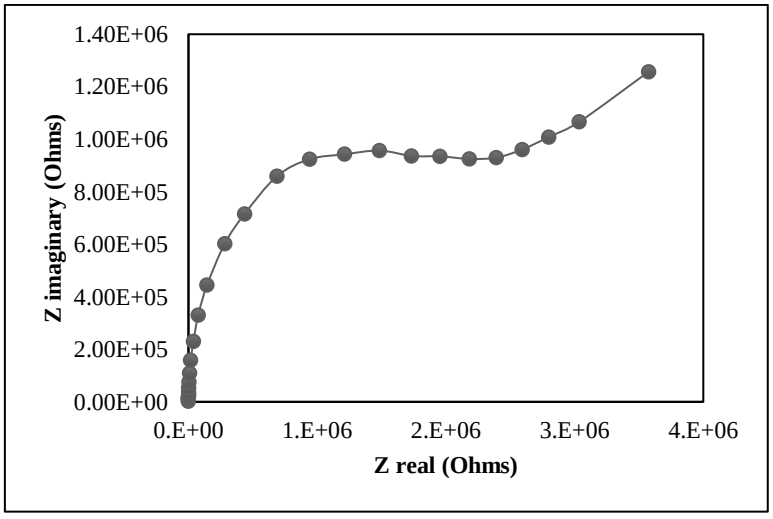

Figure 12 : Nyquist plot for the best ZrPA/STA composite membrane with $Z_{real} = 17.94$ ohms

The findings revealed that the proton conductivity exhibited an upward trend with an increase in the mass percentage of silicotungestic acid, until it reached an optimum level, after which it declined. The data in Figure 13 displays the various proton conductivity values in relation to the mass percentage of STA. The Figure indicates that the highest proton conductivity of 2.23×10^{-3} S/cm was obtained at a mass percentage of 75% silicotungstic acid. The results were consistent with what was mentioned in the literature; the composite membrane of silicotungstic acid doped in polybenzimidazole (SiWA/PBI) showed a proton conductivity of 1.2×10^{-3} S/cm [82].

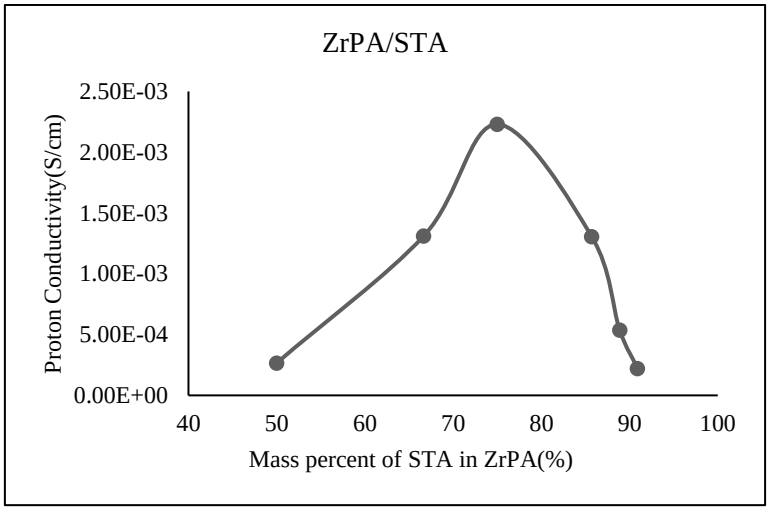

Figure 13 : Mass percentage vs conductivity for ZrPA/STA.

The addition of silicotungstic acid (STA) to zirconium phytate results in an increase in proton conductivity for several reasons. Firstly, the acidic nature of STA aids in the movement of protons through the membrane by donating acidic protons to water molecules in the membrane, thereby allowing them to move more easily. Additionally, the high density of acidic protons in silicotungstic acid facilitates the formation of strong hydrogen bonds with water molecules, which can stabilize the proton transport pathway and prevent the formation of water clusters that may hinder proton mobility [73]. Secondly, the interaction between STA and the polymer matrix of the PTFE results in the formation of a composite material that exhibits enhanced proton conductivity [94]. Finally, the unique structure of HPAs, which consists of metal atoms encircled by oxygen atoms, forms a cage-like structure that can promote proton hopping (Grotthuss mechanism) between the metal atoms, thereby leading to improved proton conductivity.

Overall, the high acidity and unique structure of HPAs make them promising materials for improving proton conductivity in PEMFCs.

4.2. ZrPA/PEG and ZrPA/STA /PEG composite membranes

PEG (Polyethylene Glycol) is a water-soluble polymer that has been studied for its potential to improve the proton conductivity of (PEMFCs). It has been investigated with both zirconium phytate and composite membrane ZrPA/STA forming ZrPA/PEG and ZrPA/STA/PEG composite membranes respectively. Nyquist plots of the best membranes in both combinations are represented in Figure 14 and Figure 15.

The incorporation of PEG into zirconium phytate (ZrPA) has resulted in a minor enhancement in proton conductivity. Specifically, the addition of 1.7% PEG increased the proton conductivity from 6.65×10^{-4} S/cm in pure ZrPA membranes to 3.22×10^{-4} S/cm in ZrPA/PEG membrane. This conductivity is reasonable as it is in agreement with the range of the proton conductivity of the PEG composite membranes ($10^{-3} - 10^{-5}$) S/cm [111].

On the other hand, PEG addition into the ZrPA/STA composite membrane has resulted in an increase by one order of magnitude in the proton conductivity. The proton conductivity has increased from 2.23×10^{-3} S/cm for ZrPA/STA to 3.81×10^{-2} S/cm at 1.7% of PEG due to the interactions between the PEG and the STA. The combined effect of the high acidity of the silicotungstic acid and the hydrophilicity of the polyethylene glycol played a significant role in improving the proton mobility in uremembrane, thus increasing the availability of water for proton transfer.

In this research, various PEG mass percentages had utilized, and their proton conductivity was investigated, as seen in Figure 16 and Figure 17 for ZrPA/PEG and ZrPA/STA/PEG, respectively. The results showed that increasing the PEG percentage by more than 1.7% led to a decrease in the proton conductivity of the membranes. The reason can be attributed to the high molecular weight of PEG, which might have contributed to the conductivity decrease by reducing the conductivity of the ionomers, ultimately leading to an increase in proton transport resistance [112].

In conclusion, it should be noted that while PEG can improve the proton conductivity of PEMFCs by improving the level of hydration and reducing the need of external source of humidification, it can also have some negative effects on the

performance of the cell. For example, it can reduce the mechanical strength of the membrane and can lead to an increase in the methanol crossover in DMFCs. Therefore, the amount of PEG added to the membrane needs to be carefully optimized to balance the benefits and drawbacks of its incorporation.

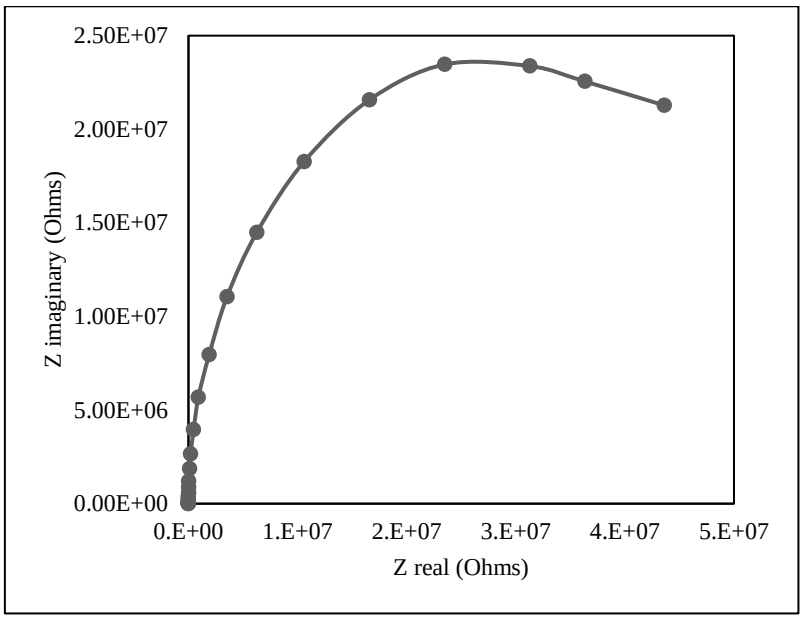

Figure 14: Nyquist plot for pure ZrPA/PEG membrane with $Z_{real} = 122$ Ohm.

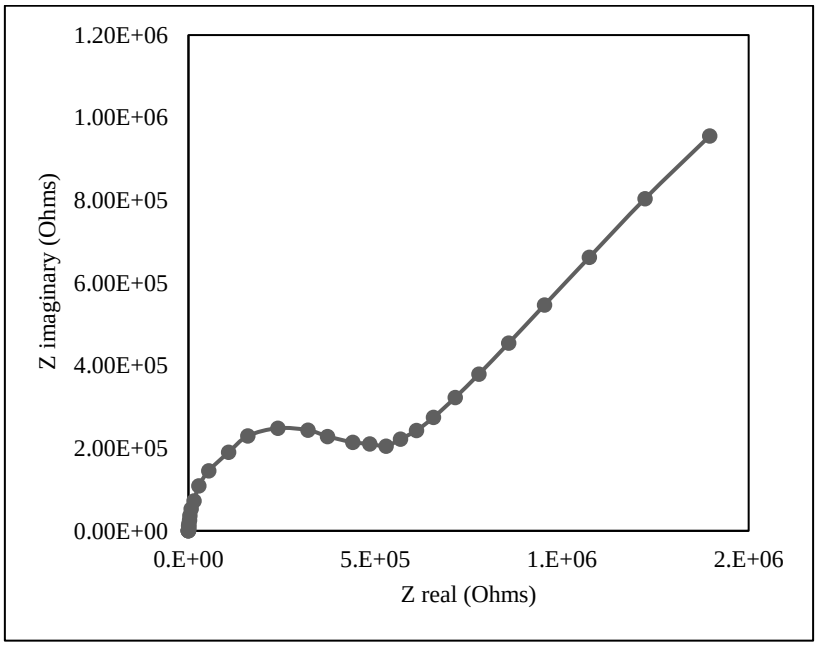

Figure 15: Nyquist plot for pure ZrPA/STA/1.7 wt%PEG membrane with $Z_{real} = 2.062$ Ohm.

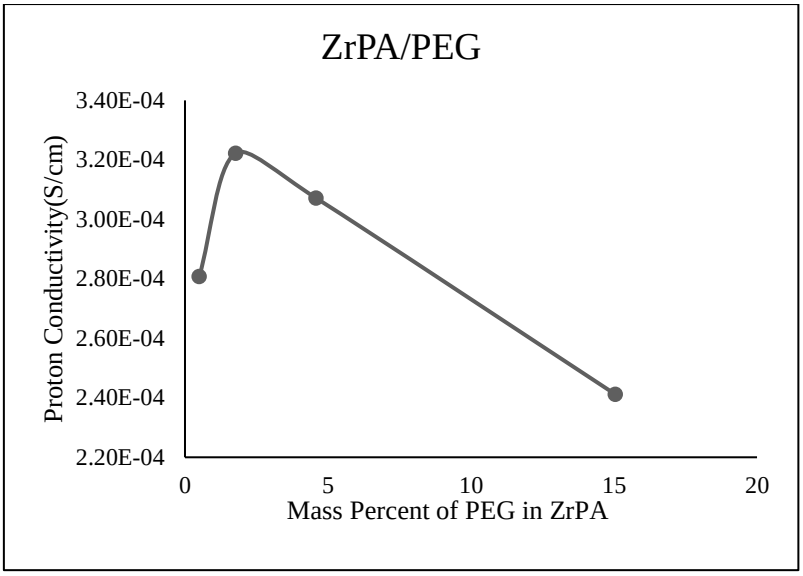

Figure 16: Mass percentage vs conductivity for ZrPA/PEG.

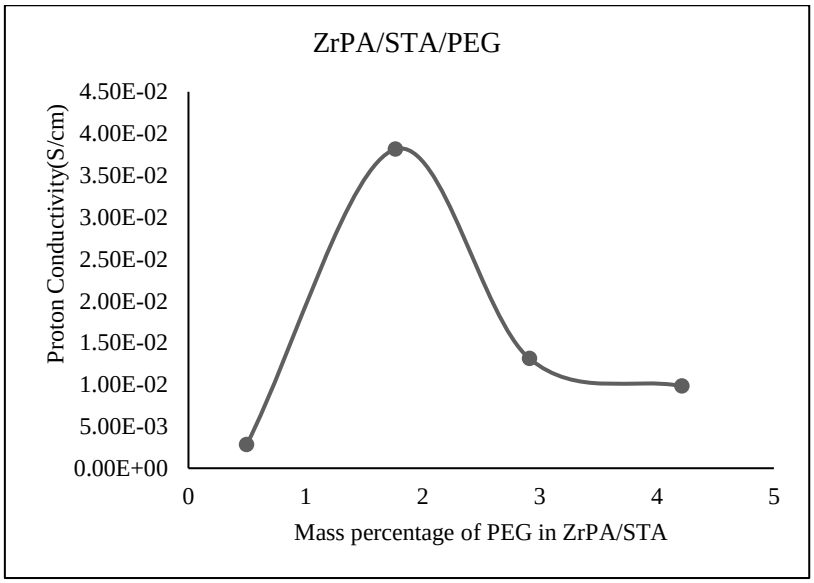

Figure 17: Mass percentage vs conductivity for ZrPA/STA/PEG.

4.3. ZrPA/ILs & ZrPA/STA/PEG/ILs composite membranes

Ionic liquids had been extensively used in PEMFCs membranes due to their high impact on the proton conductivity enhancement. In this study two imidazolium based ionic liquids were employed, 1-Hexyl-3- methylimidazolium tricyanomethanide [HMIM][$C_4N_3^-$] and 1-Ethyl-3-methylimidazolium bis(trifluoromethyl sulfonyl) imide [EMIM][BTI]. Their effect was investigated with both ZrPA membranes and ZrPA/ STA/PEG composite membranes.

The addition of 1-Hexyl-3- methylimidazolium tricyanomethanide [HMIM][$C_4N_3^-$] into the ZrPA membranes has shown a significant increase of the protonic conductivity in both the ZrPA/[HMIM][$C_4N_3^-$] and ZrPA/STA/PEG/[HMIM][$C_4N_3^-$] modified membranes. Firstly, the incorporation of [HMIM][$C_4N_3^-$] to the pure ZrPA has been investigated. The results showed that the resistance has decreased from 139.09 ohms for pure ZrPA to 8.059 ohms as seen in Figure 18. That has resulted in a raise by one order of magnitude of the conductivity (4.88×10^{-3} S/cm) upon the addition of 18.6% mass [HMIM][$C_4N_3^-$] to pure ZrPA. Figure 19 shows the different mass percentages of [HMIM][$C_4N_3^-$] that has been utilized. It is noticed that the proton conductivity has increased slightly then decreased, while maintaining the same order of magnitude. These findings are in agreement with what was mentioned in literature. As the imidazolium based ionic liquids usually possess proton conductivity of 10^{-3}S/cm [113].

Secondly, different ILs mass percentages ranging from 3% to 8% was investigated with ZrPA/STA/PEG membranes as can be seen in Figure 20. The results displayed a significant enhancement of the proton conductivity upon the addition of 5.86% mass percent of [HMIM][$C_4N_3^-$] into the ZrPA/STA/PEG composite membrane. As it gave a low bulk resistance of (0.39 ohms) as illustrated in Figure 21, which is equivalent to 0.1 S/cm. This composite membrane provided the same conductivity of Nafion's. Many recent studies showed the same enhancement upon the addition of this ionic liquid into different combination. In 2021, a research done by Ka'ki et al [114] demonstrated that the addition of [HMIM][$C_4N_3^-$] to calcium phosphate has raised the ionic conductivity from 9.58×10^{-4} S/cm to 0.1 S/cm. Another study [115] of lignin/ZrP/[HMIM][$C_4N_3^-$] confirmed that the incorporation of [HMIM][$C_4N_3^-$] has the ability to increases the conductivity to 0.1 S/cm.

This improvement could be attributed to the chemical structure of the protic ionic liquid, which enhances the hydrogen bonding. The anionic part of the ionic liquid [$C_4N_3^-$] has high affinity of forming hydrogen bonds with water molecules. This increases the proton transfer space which leads to better hopping process of hydrogen protons [H^+]. Another reason, the hydrophilic nature of the IL might increase the formation of more hydrogen bonds by absorbing more moisture. This can provide more paths for proton transfer among the water molecules [116] .

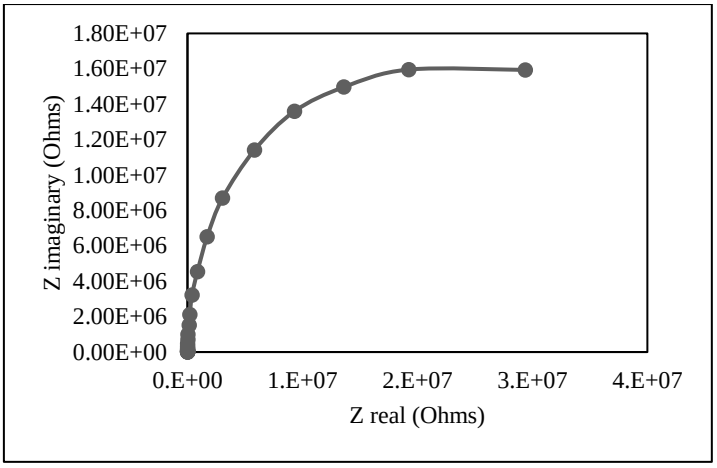

Figure 18: Nyquist plot for pure ZrPA/[HMIM][$C_4N_3^-$] with $Z_{real} = 8.059$ Ohm.

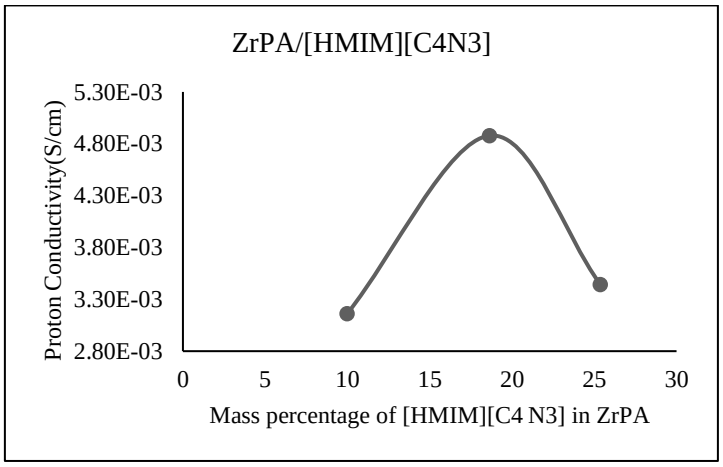

Figure 19: Mass percentage vs conductivity for ZrPA/[HMIM][$C_4N_3^-$].

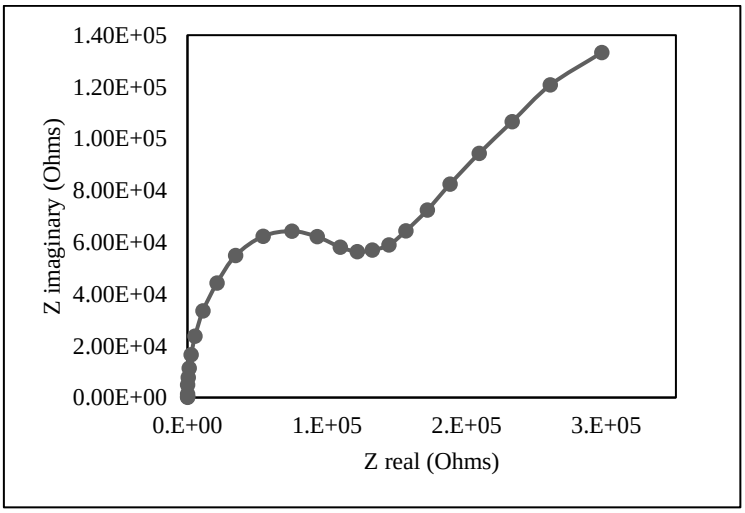

Figure 20: Nyquist plot for ZrPA/STA/PEG/5.86 wt%[HMIM][$C_4N_3^-$] with $Z_{real} = 0.39$ Ohm.

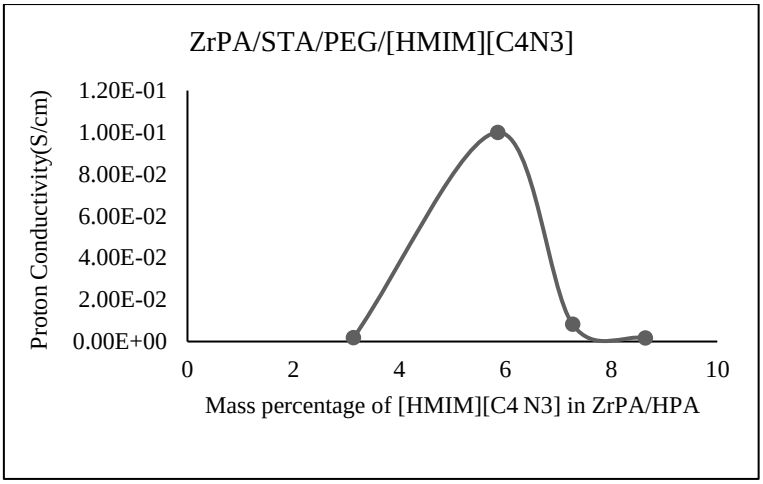

Figure 21: Mass percentage vs conductivity for ZrPA/STA/PEG/[HMIM][$C_4N_3^-$].

The other ionic liquid [EMIM][BTI] also showed an enhancement in the proton conductivity of ZrPA. However it showed lower proton conductivity with ZrPA/STA/PEG composite membrane compared to the [HMIM][$C_4N_3^-$]. In the first case, the proton conductivity has increased to 1.68×10^{-3} S/cm when 20% of ionic liquid was added to the pure ZrPA. This could be explained by the intermolecular interaction between the zirconium phytate and the [EMIM][BTI] which led to the formation of hydrogen bonds that facilitates the proton movement. The findings are consistent with the proton conductivity of imidazolium-based proton conductivity [113].

On the other hand, the conductivity of ZrPA/STA/PEG/[EMIM][BTI] has slightly decreased to 9.88×10^{-3} S/cm upon the introduction of the ionic liquid to the membrane. The reduction in conductivity values can be attributed to the increase of the viscosity of the ionic liquid due to the increase of the ionic size part [BTI]. As a result, the cohesion energy will increase, which might lead to a significant reduction in the electrostatic attraction [117]. The other reason is the low hydrophilicity of [EMIMI][BTI] which decreases the affinity of the ionic liquid to form strong hydrogen bonding with ZrPA/STA/PEG.

The resistance data of both ZrPA/[EMIMI][BTI] and ZrPA/STA/PEG/[EMIMI][BTI] modified membranes are displayed in Figure 22 and Figure 23 respectively. In the study of this ionic liquids, various masses had been used and their values vs their proton conductivity are presented in Figure 24 and Figure 25.

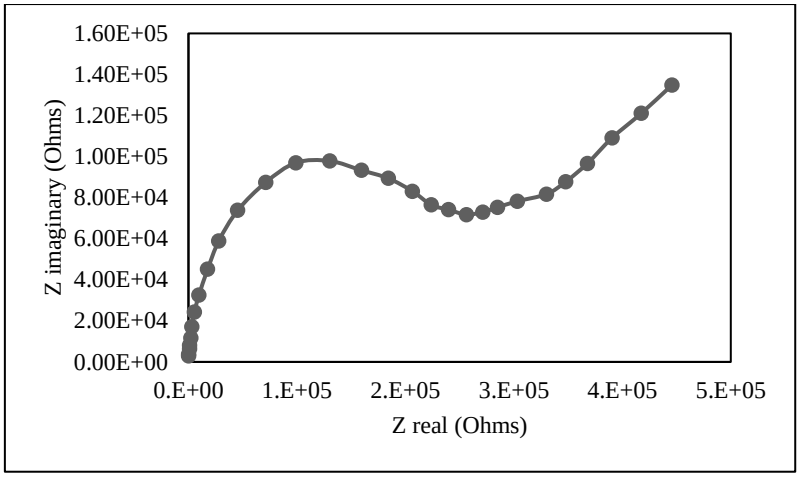

Figure 22: Nyquist plot for pure ZrPA/[EMIM][BTI] with $Z_{real} = 24$ Ohm.

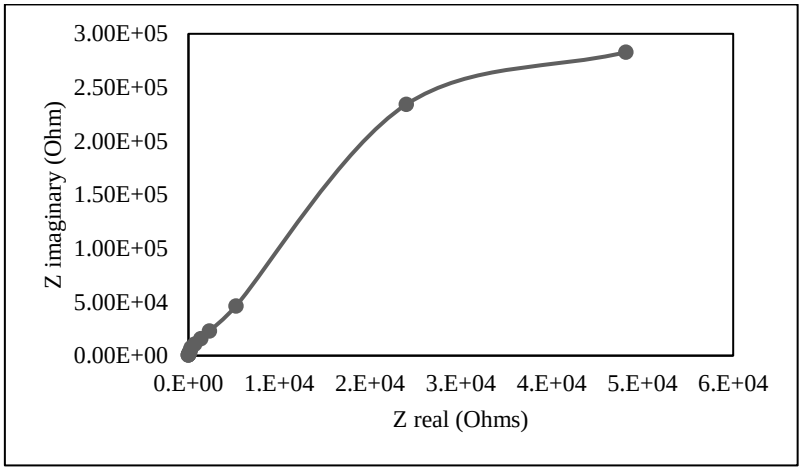

Figure 23: Nyquist plot for ZrPA/STA/PEG/6.17 wt%[EMIM][BTI] with $Z_{real} = 4.216$ Ohm.

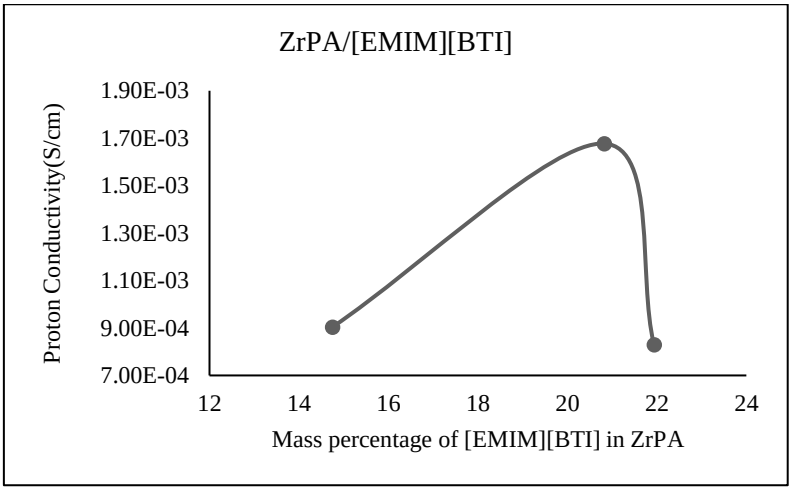

Figure 24: Mass percentage vs conductivity for ZrPA/[EMIM][BTI].

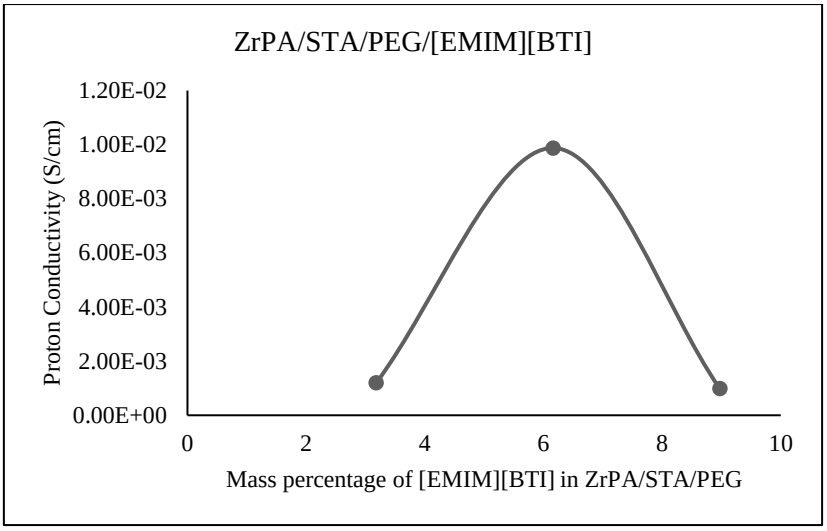

Figure 25: Mass percentage vs conductivity for ZrPA/STA/PEG/[EMIM][BTI].

In summary, table (3) provides the best conductive membranes in each combination accompanied with its resistance and proton conductivity.

Table 3: The resistance with its corresponding conductivity of the best conducting membranes in each combination.

Composite Membrane	**Resistance (Ohm)**	**Proton Conductivity (S/cm)**
ZrPA (pure)	139.09	6.65×10^{-4}
ZrPA/STA	17.94	2.23×10^{-4}
ZrPA/PEG	122	3.22×10^{-4}
ZrPA/STA/PEG	2.062	3.81×10^{-2}
ZrPA/[HMIM][$C_4N_3^-$]	8.059	4.88×10^{-3}
ZrPA/STA/PEG/5.86 wt%[HMIM][$C_4N_3^-$]	0.39	1.00×10^{-1}
ZrPA/[EMIM][BTI]	24.09	1.68×10^{-3}
ZrPA/STA/PEG/6.17 wt%[EMIM][BTI]	4.216	9.88×10^{-3}

Chapter 5. Discussion of Characterization results

In this chapter, the characterization tests ranging from EIS, TGA, FTIR, SEM, EDX, XRD, and water uptake analysis were performed. The results discussed the morphology as well as the crystalline structure of the best conductive membranes. In addition, the proton conductivity at elevated temperature (150°C) was performed.

5.1. Proton Conductivity at High-Temperature

The main goal of this comprehensive research is the investigation of the proton conductivity of the synthesized membranes at elevated temperature (150°C). In regards, the ITS machine accompanied with the potentiostant were used to test the conductivity for the best conductive membranes; ZrPA/STA/PEG, ZrPA/ STA/PEG/[HMIM][$\mathbf{C_4N_3^-}$], and ZrPA/STA/PEG/[EMIM][BTI]. The membranes were cut and fixed in the glove box, then placed inside the CESH. After that, the proton conductivity was measured using the EIS over the temperature range 25-150°C. The resistance of the corresponding membranes accompanied with their proton conductivity are displayed in table 4 and Figure 26. IL1 refers to 1-Hexyl-3- methylimidazolium tricyanomethanide [HMIM][$C_4N_3^-$], while IL2 refers to 1-Ethyl-3-methylimidazolium bis(trifluoromethyl sulfonyl) imide [EMIM][BTI].

Table 4 and Figure 26 display the resistance and the conductivity of each composite membrane. It is observed that all membrane's conductivity has dropped at least by one order of magnitude. For ZrPA/STA/PEG modified membrane, the proton conductivity has reduced by one order of magnitude from 3.8×10^{-2} S/cm at room temperature to 1.36×10^{-3} S/cm at 150°C. On the other hand, ZrPA/STA/PEG/IL1 showed a significant decrease in the conductivity by two orders of magnitudes, as it reached 6.55×10^{-3} at high temperature. Moreover, the ZrPA/STA/PEG/IL2 showed a stable behaviour in its proton conductivity over the entire range of temperature (25-150) °C. It has maintained a constant order of magnitude (10^{-3}). However, their performance is considered better than the standard Nafion, which gave a low conductivity at 30°C & relatively low humidity ($1.4 \times 10^{-4}\ S/cm$) [ref].

The high conductivity at HT-operation is attributed to the acidic backbone structure of the silicotungstic acid, as it has the ability to retain water molecules, hence

providing path for protons transfer. The findings were found to be consistent with the literature. The silicotungstic acid has given high proton conductivity in most of its composite membranes at elevated temperatures. For instance, doping 50% SIWA in SiO_2/PBI composite membrane has resulted in 1.2×10^{-3} S/cm at 160°C and completely hydrous conditions (100% RH) [83]. Another research revealed that 9.6 wt% of SIWA in SPEEK provided 0.0013 S/cm at 96°C [118].

Table 4: Effect of temperature of the best conducting membranes over temperature range (25-150) °C.

Temperature (°C)	**ZrPA/STA/PEG**		**ZrPA/STA/PEG/IL1**		**ZrPA/STA/PEG/IL2**	
Resistance/ Conductivity	Ohm	S/cm	Ohm	S/cm	Ohm	S/cm
25	1.035	3.80E-02	0.390	1.00E-01	4.504	8.73E-03
35	2.228	1.76E-02	1.103	3.56E-02	4.755	8.27E-03
45	3.956	9.94E-03	5.794	6.78E-03	6.927	5.67E-03
55	4.617	8.51E-03	9.071	4.33E-03	7.625	5.16E-03
65	6.084	6.46E-03	12.050	3.26E-03	8.426	4.67E-03
75	8.302	4.73E-03	14.260	2.76E-03	8.657	4.54E-03
80	10.800	3.64E-03	14.870	2.64E-03	8.512	4.62E-03
85	15.470	2.54E-03	14.390	2.73E-03	8.543	4.60E-03
90	11.540	3.41E-03	9.961	3.95E-03	9.807	4.01E-03
100	14.339	2.74E-03	17.620	2.23E-03	11.190	3.51E-03
110	23.010	1.71E-03	5.710	6.88E-03	13.140	2.99E-03
120	25.110	1.57E-03	9.570	4.11E-03	17.000	2.31E-03
130	28.650	1.37E-03	5.129	7.66E-03	18.200	2.16E-03
140	28.830	1.36E-03	5.711	6.88E-03	21.390	1.84E-03
150	29.000	1.36E-03	6.000	6.55E-03	29.070	1.35E-03

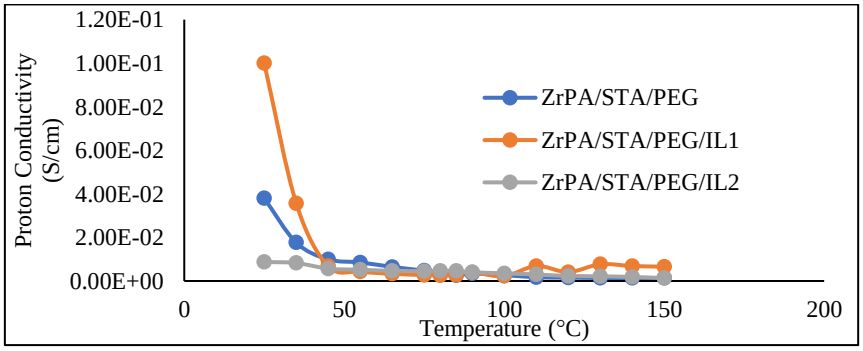

Figure 26: Effect of temperature on the best conductive membranes.

5.2. Thermogravimetric analysis (TGA)

Thermogravimetric analysis was applied to the best conductive composite membranes to investigate their thermal stability as well as their weight loss and compare it to the pure PTFE support sheet. The selected samples were exposed to temperature from 27°C to 900°C in the presence of Nitrogen as inert and at a heating rate of 20°C/min. The process took a round 45 minutes. Figure 27 illustrates the TGA for the pure PTFE and the modified ZrPA membranes with silicotungstic acid, PEG, and the two ionic liquids.

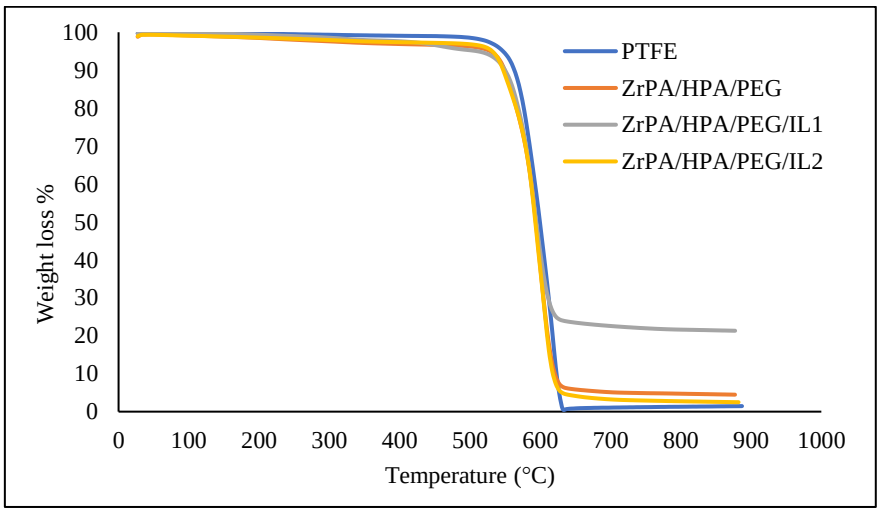

Figure 27: TGA for pure PTFE, ZrPA/STA/PEG, ZrPA/STA/PEG/IL1, ZrPA/STA/PEG/IL2 membranes.

By looking at Figure 27, it is observed that less than 1% weight was lost at 27-430°C for pure PTFE due to the loss of water molecules. A large weight drop was observed around 640°C due to the decomposition of the PTFE support [119], followed by a maximum degradation at 900°C. TGA analysis for the modified ZrPA/STA/PEG showed the same performance as the pure PTFE below 100°C. Then, it lost a round 3% of its mass weight from 100°C to 380°C, followed by a dramatic decrease (34%) at 600°C, and a total decomposition at 900°C. this can be attributed to the loss of the interlayer water bound [72]. ZrPA/STA/PEG/IL1 and ZrPA/STA/PEG/IL2 on the other hand, lost 10% of their corresponding weight at 547°C. However, at 630°C, ZrPA/STA/PEG/IL1 showed more thermal stability than ZrPA/STA/PEG/IL2. Its mass weight has decreased more rapidly by 5 times than ZrPA/STA/PEG/IL1. AT 900°C, only 2.4% was remaining of ZrPA/STA/PEG/IL2, compared to 21.3% of

ZrPA/STA/PEG/IL1. Hence, IL1 ([HMIM][$C_4N_3^-$]) exhibited significant thermal stability in comparison to IL2 ([EMIM][BTI]). The reason can be attributed to the water retention properties of IL1.

In general, research has shown that using silicotungstic acid along with PEG and ILs to modify pure ZrPA sample has improved their ability to absorb water, hence, enhancing their thermal stability. TGA curves indicate that modified membranes display outstanding water absorption properties, with very little weight loss up to 150°C when compared to the pure ZrPA without any additives [72] . This is consistent with the proton conductivity results. Furthermore, the modified materials created multiple hydrogen bonds with STA, PEG and ILs. Therefore, ZrPA/STA/PEG/[HMIM][$C_4N_3^-$] and ZrPA/STA/PEG/[EMIM][BTI] demonstrated excellent thermal stability, with minimal weight loss, making them suitable for high-temperature fuel cell applications.

5.3. Fourier Transform Infrared Spectroscopy (FTIR)

FTIR analysis was performed on synthesized membranes to investigate the chemical bond interactions and the functional groups in pure ZrPA membrane and the modified ZrPA membranes with STA, and PEG. FTIR was also conducted on the best conductive membranes ZrPA/STA/PEG/ILs. The FTIR spectrum for pure ZrPA and the ZrPA/STA, ZrPA/PEG, and ZrPA/STA/PEG composite membranes are depicted in Figure 28 and Figure 29, respectively.

The FTIR spectrum shown in Figure 28 of ZrPA displays various absorption peaks. The peaks at 3838, 3728, and 3267 $cm^{-1}$are related to the O-H hydroxyl group present in phytic acid, which interacts with other hydroxyl groups and P=O bonds through hydrogen bonding [72]. The peak at 2991 corresponds to the C-H stretching vibration, while the peak at 1736 corresponds to the H-O-H interlayer bond water [121]. The peaks at 1547 and 1456 cm^{-1} represent P=O in the phosphonic acid group. Furthermore, the sharp peaks at 1208 and 1145 cm^{-1} correspond to the C-F asymmetric stretching vibration, which indicates the presence of the PTFE membrane base matrix [122]. The sharp peak at 1001 is attributed to the C-P-O stretching vibration. Moreover, the chelation of Zr^{4+} is indicated by the lower wavelength numbers (773-423 cm^{-1}) [72]. The presence of PTFE peaks is noted in all membranes, along with low wavenumbers indicating the immobilization of Zirconium ion (Zr^{4+}).

The ZrPA/PEG spectrum in Figure 29 displays similar peaks to ZrPA, except for the 3268-3841cm^{-1} band, which is wider and less intense. This can be attributed to the interaction between PEG and ZrPA. Moreover, it is noticed that the absorption peak at 3741 cm^{-1} has been eliminated and become flat, which indicate the introduction of more O-H group upon the addition of STA to ZrPA. On the other hand, the H-O-H absorption peak at 1721 cm^{-1} has become broader and wider, possibly indicating the absorption of more water molecules within the membrane [123]. The ZrPA/STA/PEG spectrum is dominated by the effect of STA addition, as it is much similar to the ZrPA/STA spectra, likely due to the small amount of PEG added compared to STA added amount. However, the absorption peak at 1587 cm^{-1} indicates the intercalation of PEG within the ZrPA/STA composite membrane. The disappearance of the 3267 cm^{-1} peak in the ZrPA/STA/PEG membrane suggests intercalation between the STA and PEG molecules within the ZrPA interlayer. The broader region in ZrPA/STA and ZrPA/STA/PEG at absorption peak 975 cm^{-1} is attributed to Si-O bond in silicotungstic acid [124].

Figure 30 demonstrates the effect of immobilization of ionic liquids within the ZrPA/STA/PEG membrane. It is observed that both ILs spectra are relatively identical. The absorption peaks at 504-914 cm^{-1} have become sharper and more intense in ZrPA/STA/PEG/ILs when compared to the ZrPA/STA/PEG. This can be attributed to the intercalation of ILs within the ZrPA structure. The shoulder at 1100 cm^{-1} in ZrPA/STA/PEG/[HMIM][$C_4N_3^-$] is due to C-OH bond. It is an indication of more water molecules absorption within the membrane. Moreover, the broader band at 1391 cm^{-1} also illustrates the C-OH bending mode [125]. Additionally, the absorption peak at 1600 cm^{-1}and the wide band at 2096 cm-1 are attributed to the C-H bending vibrational modes [114]. The stretching band at 3267 cm-1 and the 3734 cm-1 peak are due to the water absorption [126]. In ZrPA/STA/PEG/[EMIM][BTI] the shoulder band at 1323 cm^{-1} is assigned to the C-F bond, which is due to the introduction of [EMIM][BTI] ionic liquid into the membrane matrix. The H_2O molecules absorption has also been seen in [EMIM][BTI] at 3028 cm^{-1}. In general, the FTIR analysis of all membranes revealed similar spectrum trends. However, the C-OH peaks were more prominent and higher in the membranes containing ILs, which confirms their high-water content and ionic conductivity.

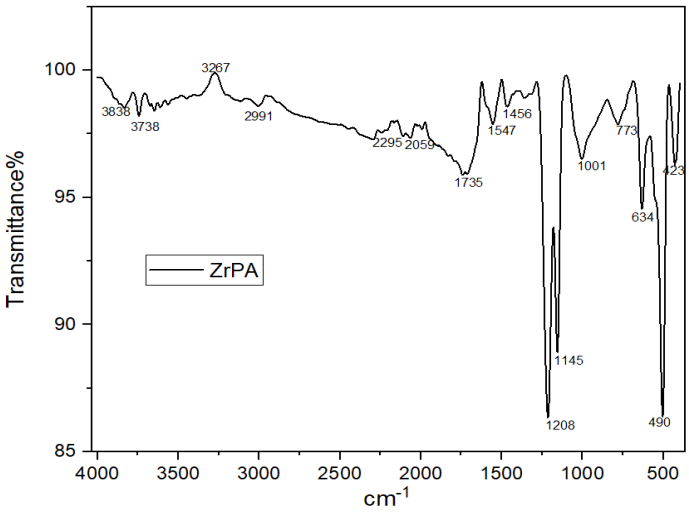

Figure 28: FTIR spectra for ZrPA membranes.

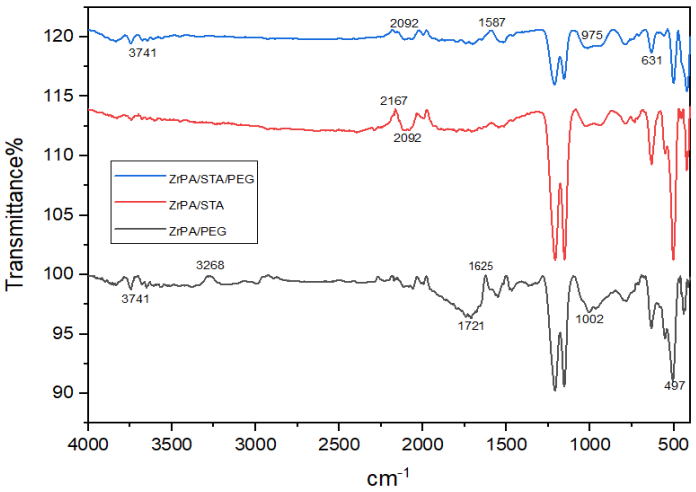

Figure 29: FTIR spectra for ZrPA/PEG, ZrPA/STA, & ZrPA/STA/PEG membranes.

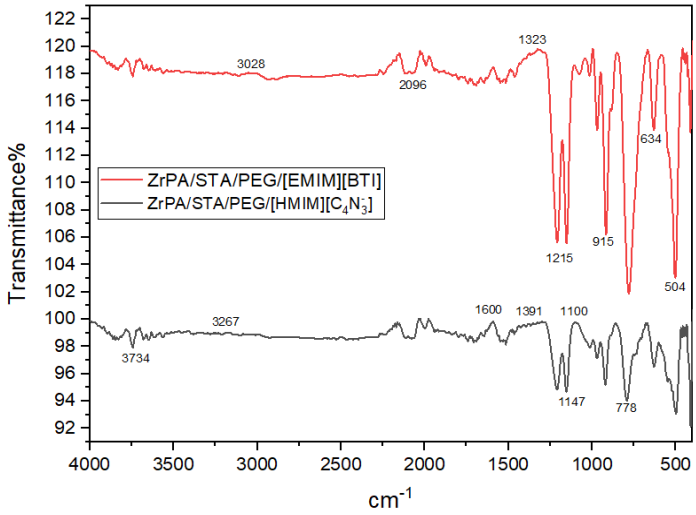

Figure 30: FTIR spectra for ZrPA/STA/PEG/[HMIM][$C_4N_3^-$] & ZrPA/STA/PEG/[EMIM][BTI] composite membranes.

5.4. Scanning Electron Microscopy (SEM)

An AMRAY scanning electron microscope (SEM) was utilized to assess the consistency of additive dispersion in the membrane, as well as the size of the additive particles/agglomerates. SEM imaging was conducted at various magnifications, using an electron beam energy of 20 kV. To prepare the samples, small membrane pieces were cut and placed onto sample stubs covered in carbon tape. A thin layer of Au-Pd was sputtered onto the sample to enhance electrical conductivity and reduce artifacts caused by sample charging.

Figure 31, Figure 32, Figure 33, and Figure 34 depict the surface topographies of different membrane samples. Figure 31 displays the surface morphology of ZrPA/STA, revealing irregularly distributed nanoparticles formed due to the interaction between ZrPA and STA. In Figure 32, it was observed that adding PEG to the ZrPA/STA composite membrane caused particle agglomeration, which can be attributed to the high viscosity of PEG. Moreover, it was noticed that the immobilization of ionic liquids, which are commonly referred to as structure-directing agents, has significantly decreased the particle size, leading to a substantial enhancement in the available surface area of the membrane's structure [127]. The incorporation of ionic liquids has also improved the nucleation among the ZrPA/STA/PEG layer structure, leading to a better crystalline structure compared to the unmodified membrane. The SEM micrographs of the most conductive membrane, ZrPA/STA/PEG//[HMIM][$C_4N_3^-$], are presented in Figure 33. The images reveal that the formed particles are predominantly spherical in shape and are distributed as either individual units or agglomerates. It is observed that particle size has decreased dramatically upon the addition of ILs from microns in unmodified ZrPA/STA/PEG membranes to (200-500) nm [115]. These nanoparticles exhibit favourable interactions between the PTFE and the added materials, as it has resulted in an increase in the surface area of the composite membrane, which increased the proton pathways within the membrane matrix. These results confirm the high proton conductivity. Furthermore, Figure 34 shows the top view of ZrPA/STA/PEG/[HMIM][BTI], where the nanoparticles exhibit an irregular fusiform crystal shape.

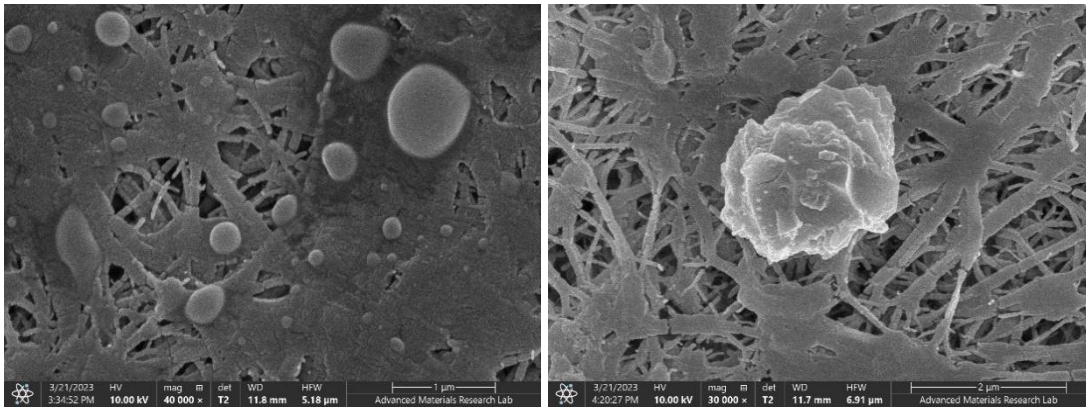

(a) (b)

Figure 31: SEM images for ZrPA/STA at magnifications of (a) 40000X, (b) 30000X.

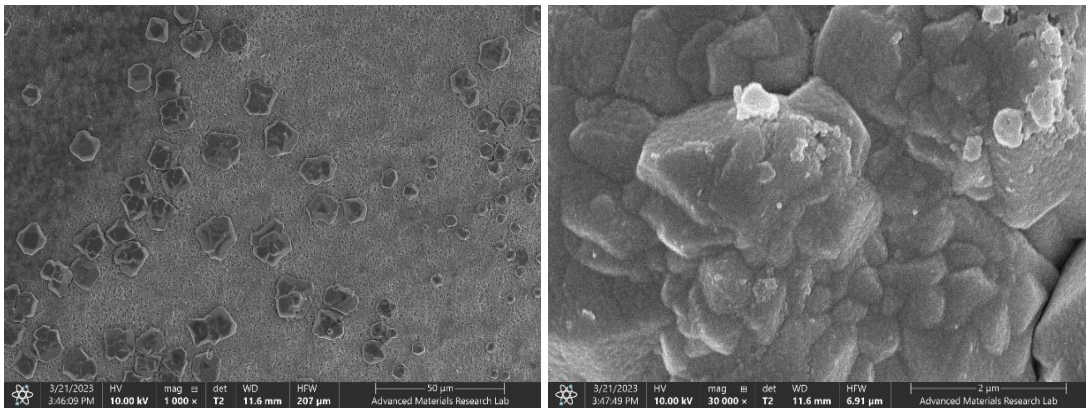

(c) (d)

Figure 32: SEM images for ZrPA/STA/PEG at magnifications of (c) 1000X, (d) 30000X.

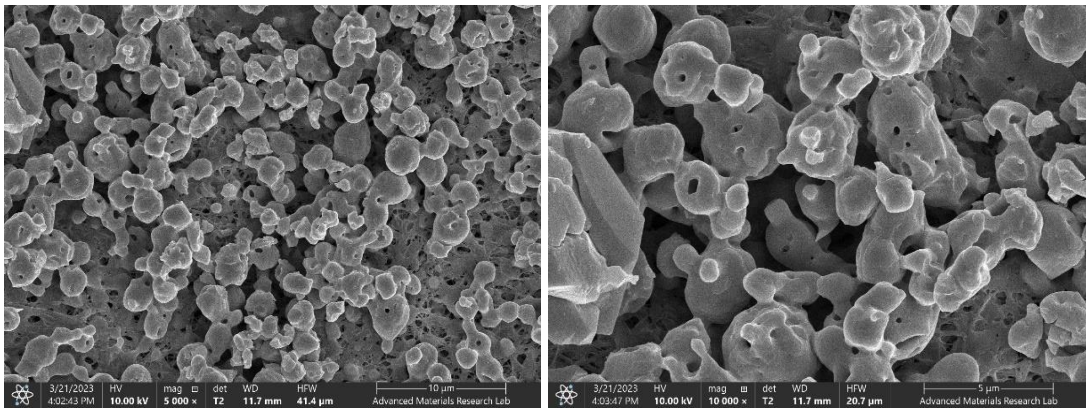

(e) (f)

Figure 33: SEM images for ZrPA/STA/PEG/[HMIM][$C_4N_3^-$] at magnifications of (e) 5000X, (f)10000X.

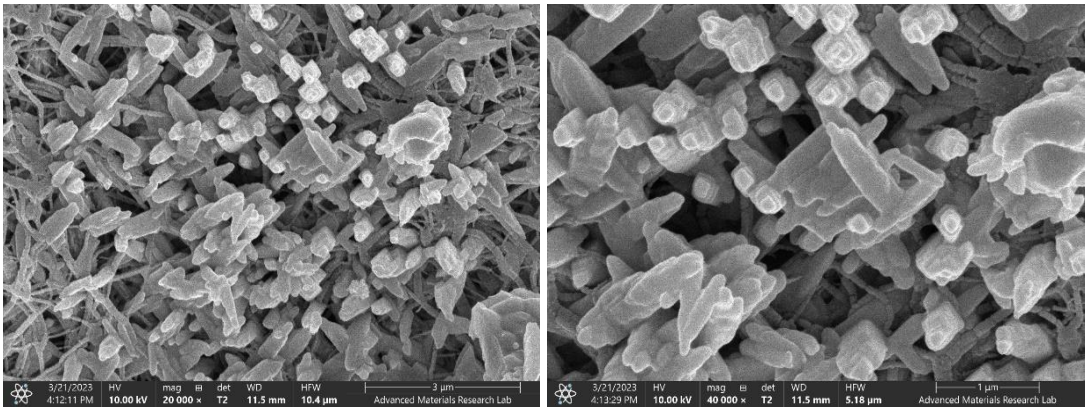

(g) (h)

Figure 34: SEM images for ZrPA/STA/PEG/[EMIM][BTI] at magnifications of (g) 20000X, (h) 40000X.

5.5. Energy Dispersive X-ray (EDX)

To perform a quantitative elemental analysis, EDX was conducted in combination with SEM for the best conductive membranes. EDX was studied in different regions of these samples, with the ionization energy displayed on the abscissa and the counts indicated on the ordinate of the EDX spectrum. The corresponding peaks are illustrated in Figure 35, Figure 36, and Figure 37.

In ZrPA/STA/PEG composite membrane, the atomic percentages for W, C, O, Zr, and Si were found to be 67.1%, 16.1%, 15.1%, 0.9%, and 0.2%, respectively. These percentages shows that tungsten, carbon, and oxygen percentages were the highest due to the addition of STA and PEG to ZrPA [72]. The addition of [EMIM][BTI] to ZrPA/STA/PEG composite is appeared clearly upon the formation of fluorine as seen in Figure 36. It is observed that the peaks of zirconium and phosphate are overlapped by the tungsten peak. This can be attributed to the high mass percentage of silicotungestic acid compared to the Zr and P masses. The high elemental percentage of carbon in all membranes is attributed to the polyethylene glycol addition.

The oxygen level in ZrPA/STA/PEG/[HMIM][$C_4N_3^-$] are found to be double the oxygen composition in ZrPA/STA/PEG/[EMIM][BTI]. This confirms the higher conductivity results of ZrPA/STA/PEG/[HMIM][$C_4N_3^-$] compared to ZrPA/STA/PEG/[EMIM][BTI]. As this indicates the increase in hydrogen bonding in structures. In addition, the high percentage of W increases the hydrogen bonding due to the four unpaired electrons in each tungsten atom.

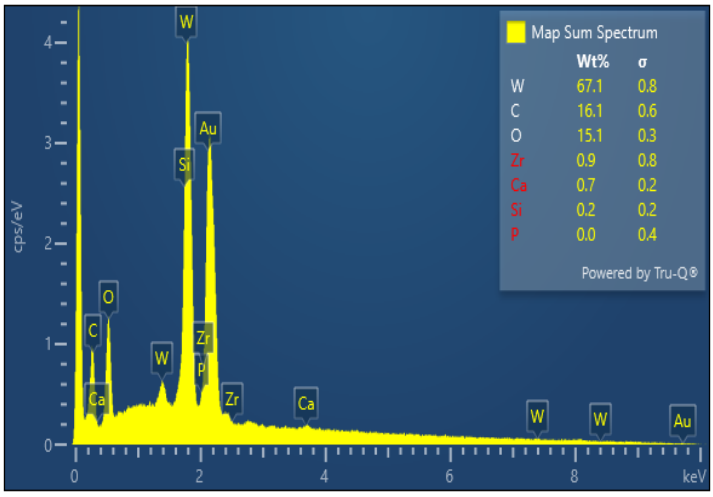

Figure 35: EDX for ZrPA/STA/PEG.

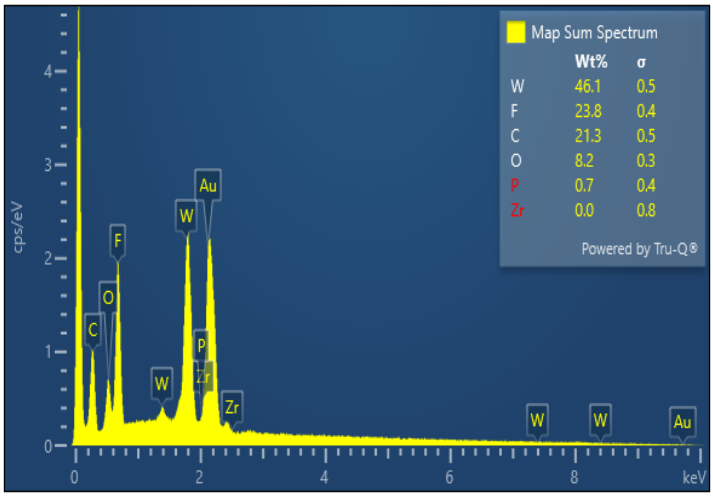

Figure 36: EDX for ZrPA/STA/PEG/[EMIM][BTI].

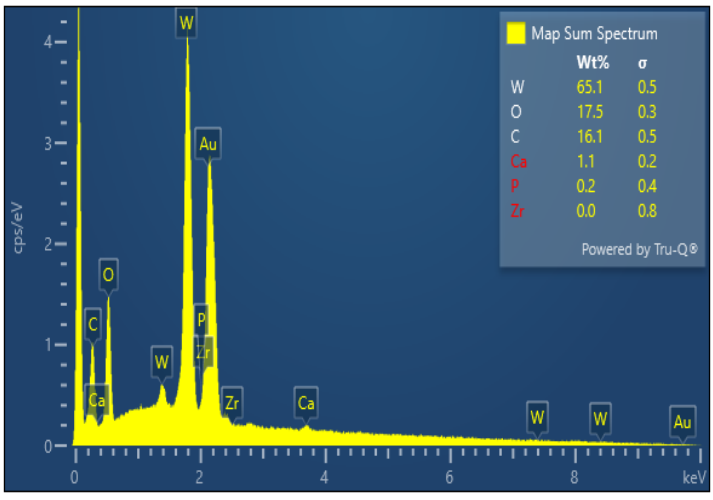

Figure 37: EDX for ZrPA/STA/PEG/[HMIM][$C_4N_3^-$].

5.6. X-Ray Diffraction (XRD)

The crystalline structure of the synthesized membranes was investigated using the XRD analysis. XRD was performed on the best conductive composite membranes and was compared to the pure ZrPA sample. The XRD spectra for pure ZrPA and modified membranes are provided in Figures 38 and Figure 39, respectively.

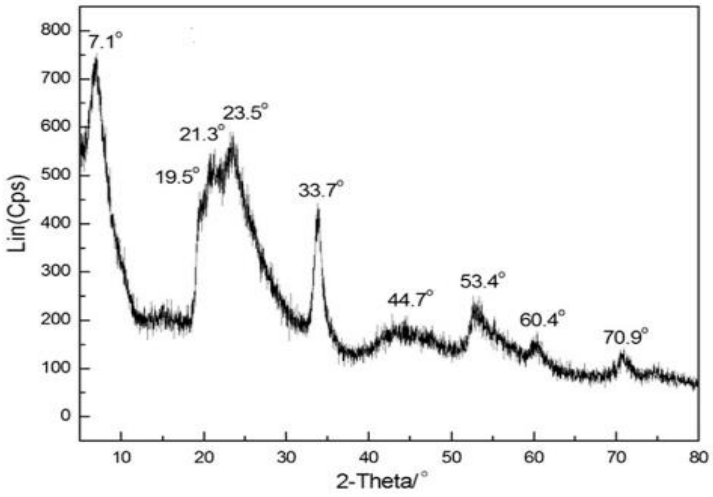

Figure 38: XRD spectra for ZrPA [72].

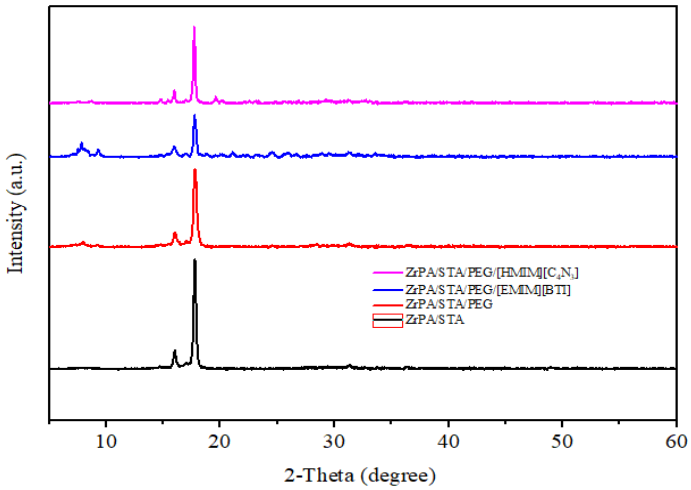

Figure 39: XRD spectra for ZrPA/STA & best conductive membranes.

In Figure 38, it is observed that the peaks possess a low sharp intensity which indicates the low crystallinity of the ZrPA membrane. This was attributed to the phytic acid crystalline structure [72]. On the other hand, the modified ZrPA membranes have demonstrated narrower peaks with sharper intensity at 18° due the PTFE support matrix. There is a strong correlation between the moisture content and the crystalline

structure of a material. When the level of crystallinity decreases, there is a corresponding rise in the amount of water intercalated within the crystal lattice [128]. The low crystallinity in the ZrPA sample illustrates the good water absorption within its layers, which supports the ZrPA protonic conductivity. The diagram obtained from X-ray diffraction shows peaks of different intensities at specific 2θ angles. By identifying the 2θ values, it is possible to obtain information about the deflection of the beams. Bragg's law [129] as seen in Eq.13 can be used in the calculations to determine the d-spacing between atoms in the modified samples.

$$2\,d\sin\theta = \lambda \tag{13}$$

Sharp peaks were observed in the ZrPA at 7.1°, 23.5°, 33.7°, 53.4°, and 70.9°, while the other peaks had a lower intensity. According to Bragg's law, a 12.54 Å d-spacing was found between the ZrPA interlayers. The ZrPA 2-theta values indicated that ZrPA had a fusiform crystalline structure. On the other hand, the modified ZrPA samples containing STA, PEG, and ILs had sharper peaks at 2θ values of approximately 16.5° and 18.05°. The disappearance of peaks at 23.5°, 33.7°, 53.4°, and 70.9° suggested a significant alteration in the crystalline structure, is possibly due to the intercalation and exfoliation of the guest molecules within the ZrPA structure. These results align with the FTIR findings, which showed great O-H absorption peaks, indicating the presence of water molecules within the membrane layers.

5.7. Water Uptake Analysis

The ability of the membrane to retain water molecules within its structure is referred to as its water uptake property. This characteristic is of significant importance in facilitating the movement of protons within the polymer electrolyte of a fuel cell by creating paths for proton hopping. To determine this property, the membrane is submerged in deionized water for a period of 24 hours, then dried for 4 hours in an oven. After that, the total mass of the membrane is measured before and after drying, followed by calculating the water uptake using equation (12). The water uptake analysis was carried out on the best conductive membranes, and their values were compared to those of Nafion. Table (5) displays the water content analysis for ZrPA/STA/PEG, ZrPA/STA/PEG/[HMIM][$C_4N_3^-$], ZrPA/STA/PEG/[EMIM][BTI], and Nafion. It is clearly seen that the ZrPA/STA/PEG, and ZrPA/STA/PEG/[HMIM][$C_4N_3^-$], contained

a water uptake percentage of 219.8% and 221.8% respectively. On the other hand, ZrPA/STA/PEG/[EMIM][BTI] has only showed a 67.3% water holding ability. These results as can be seen in Figure 40, are consistent with the proton conductivity results, as the ZrPA/STA/PEG, and ZrPA/STA/PEG/[HMIM][$C_4N_3^-$], provided the best ionic conductivity while the ZrPA/STA/PEG/[EMIM][BTI] showed the lowest conductivity. In comparison to Nafion-117, the new composite membranes appear to be highly promising for high temperature operations.

Table 5: Water uptake comparison between the best conductive membranes and Nafion.

Composite membrane	Water Uptake%
ZrPA/PEG/STA	**219.8%**
ZrPA/PEG/STA/[HMIM][$C_4N_3^-$]	**221.80%**
ZrPA/PEG/STA/[EMIM][BTI]	**67.30%**
Nafion-117	**19%**

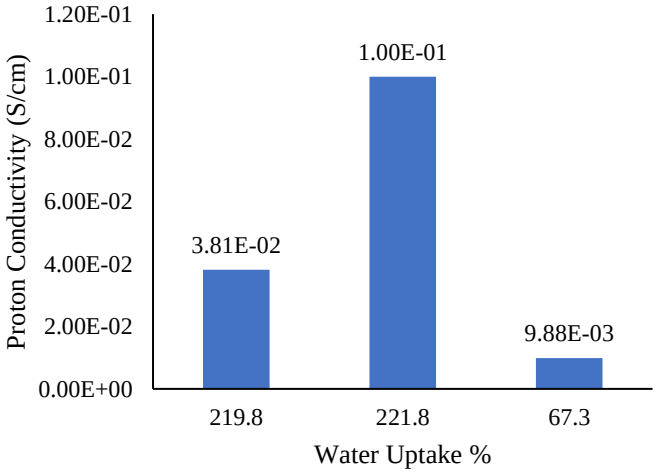

Figure 40: Proton conductivity vs water uptake for the best conductive membranes.

Overall, the synthesized composite membranes have shown the potential as candidates for HT-PEMFC operation, as confirmed by the various characterization techniques. However, further investigation is required for a better understanding of the chemical and morphological changes that occur during their synthesis. Specifically, additional XRD analysis should be performed on the starting materials and compare the results with after the synthesis. Additionally, more FTIR analysis should be conducted on the starting materials, the $ZrOCl_2$ and phytic acid before and after their reaction to

gain insight into changes in chemical bonding and functional groups. To better understand the reduction in conductivity after the high-temperature testing, it would be helpful to perform additional XRD analysis on the most conductive membranes after testing and compare the results with those obtained at room temperature.

Chapter 6. Conclusions and Future Work

6.1. Conclusions

This work reported an innovative Nafion-free, solid proton-conductive membrane, based on zirconium phytate (ZrPA) and Silicotungstic acid (STA). To enhance proton conductivity, the membrane's structure was altered with a plasticizer (PEG) and ionic liquids. The modified membranes were synthesized using the spin coating technique and were further characterized by EIS and processed at high temperatures to evaluate their proton conductivity. In addition, their thermal stability, morphology, crystallinity, elemental composition, and water retention properties were analysed using techniques such as TGA, SEM, and EDX. The membranes were synthesized by the precipitation of zirconium phytate in situ and modified with STA, PEG, and ILs. Two ionic liquids, [HMIM][$C_4N_3^-$], and [EMIM][BTI] were utilized in this study.

The proton conductivity of unmodified ZrPA was found to be 6.65×10^{-4}S/cm. The addition of STA has increased it by one order of magnitude to 2.23×10^{-3}S/cm. Further modification using PEG has increased the proton conductivity to 3.81×10^{-2}S/cm. The highest proton conductivity (0.1 S/cm) was obtained upon the addition of [HMIM][$C_4N_3^-$], which is comparable to Nafion's conductivity. In general, the addition of ionic liquids has increased the proton pathways which enhanced the proton hopping within the membrane matrix. This can be attributed to the high hydrophilicity of ionic liquids, which ultimately resulted in significant improvement of the proton conductivity.

Many characterization techniques were performed to confirm the high conductivity results. The water uptake results have shown an outstanding ability of the membrane absorbance of water, which resulted in increasing the proton conductivity as well as the durability of the membrane.

On the other hand, the SEM results have shown an increase in the surface area due to the formation of nanoparticles, which facilitates the protons transfer within the membrane matrix. In addition, the FTIR and XRD results have shown an increase in the water uptake ability upon the formation of an amorphous structure.

High temperature analysis was performed on the best conductive membranes, ZrPA/STA/PEG, ZrPA/STA/PEG/[HMIM][$C_4N_3^-$], and ZrPA/STA/PEG/[EMIM][BTI]. The results showed a dramatic decrease in the proton conductivity at least by one order of magnitude, due to the loss of water content. When compared to Nafion, the results seem better as Nafion's conductivity starts to decrease dramatically above 80°C. However, the TGA analysis has shown a great thermal stability at elevated temperatures.

In conclusion, the characterization results of the best conductive membrane ZrPA/STA/PEG/[HMIM][$C_4N_3^-$] have shown that this modified membrane can be used as alternative for the standard Nafion for high-temperature PEM fuel cell applications.

6.2. Future work and recommendations

1) Investigate another method for membranes' synthesis rather than spin coating and study their morphological structure and proton conductivity at high temperatures.
2) Investigate other types of heteropoly acids such as phosphotungistic acid and study their effect on proton conductivity.
3) Synthesize membranes with other imidazolium based ionic liquids and investigate their influence on both the thermal stability and ionic conductivity.
4) Synthesize membranes based on PBI, SPEEK and perform high temperature analysis on them.
5) Study the mechanical stability of the membranes by testing its tensile strength.
6) Study the pH effect on the membrane's proton conductivity.

References

[1] S. Khosravi H, Q. Abbas, and K. Reichmann, “Electrochemical aspects of interconnect materials in PEMFCs,” *Int J Hydrogen Energy*, vol. 46, no. 71, pp. 35420–35447, Oct. 2021, doi: 10.1016/J.IJHYDENE.2021.08.105.

[2] A. G. Olabi, T. Wilberforce, E. T. Sayed, K. Elsaid, H. Rezk, and M. A. Abdelkareem, “Recent progress of graphene based nanomaterials in bioelectrochemical systems,” *Science of The Total Environment*, vol. 749, p. 141225, Dec. 2020, doi: 10.1016/J.SCITOTENV.2020.141225.

[3] A. G. Olabi *et al.*, “Large-vscale hydrogen production and storage technologies: Current status and future directions,” *Int J Hydrogen Energy*, vol. 46, no. 45, pp. 23498–23528, Jul. 2021, doi: 10.1016/J.IJHYDENE.2020.10.110.

[4] M. Tawalbeh, A. Al-Othman, F. Kafiah, E. Abdelsalam, F. Almomani, and M. Alkasrawi, “Environmental impacts of solar photovoltaic systems: A critical review of recent progress and future outlook,” *Science of The Total Environment*, vol. 759, p. 143528, Mar. 2021, doi: 10.1016/J.SCITOTENV.2020.143528.

[5] A. H. Alami *et al.*, “Materials and logistics for carbon dioxide capture, storage and utilization,” *Science of The Total Environment*, vol. 717, p. 137221, May 2020, doi: 10.1016/J.SCITOTENV.2020.137221.

[6] M. Tawalbeh, M. Al-Ismaily, B. Kruczek, and F. H. Tezel, “Modeling the transport of CO2, N2, and their binary mixtures through highly permeable silicalite-1 membranes using Maxwell−Stefan equations,” *Chemosphere*, vol. 263, p. 127935, Jan. 2021, doi: 10.1016/J.CHEMOSPHERE.2020.127935.

[7] M. M. Mostafa, “Catastrophe Theory Predicts International Concern for Global Warming,” *Journal of Quantitative Economics*, vol. 18, no. 3, pp. 709–731, Sep. 2020, doi: 10.1007/s40953-020-00199-8.

[8] U. Lucia, “Overview on fuel cells,” *Renewable and Sustainable Energy Reviews*, vol. 30, pp. 164–169, Feb. 2014, doi: 10.1016/J.RSER.2013.09.025.

[9] O. B. Inal and C. Deniz, “Assessment of fuel cell types for ships: Based on multi-criteria decision analysis,” *J Clean Prod*, vol. 265, p. 121734, Aug. 2020, doi: 10.1016/J.JCLEPRO.2020.121734.

[10] J. Wisniak, “Historical Notes: Electrochemistry and Fuel Cells: The Contribution of William Robert Grove,” *Indian J Hist Sci*, vol. 50, no. 4, Aug. 2015, doi: 10.16943/ijhs/2015/v50i4/48318.

[11] C. Song, “Fuel processing for low-temperature and high-temperature fuel cells: Challenges, and opportunities for sustainable development in the 21st century,” *Catal Today*, vol. 77, no. 1–2, pp. 17–49, 2002, doi: 10.1016/S0920-5861(02)00231-6.

[12] W. R. Grove, “ XXIV. On voltaic series and the combination of gases by platinum ,” *The London, Edinburgh, and Dublin Philosophical Magazine and Journal of Science*, vol. 14, no. 86–87, pp. 127–130, Feb. 1839, doi: 10.1080/14786443908649684.

[13] J. M. Andújar and F. Segura, “Fuel cells: History and updating. A walk along two centuries,” *Renewable and Sustainable Energy Reviews*, vol. 13, no. 9, pp. 2309–2322, Dec. 2009, doi: 10.1016/J.RSER.2009.03.015.

[14] C. Y. Wong *et al.*, “Additives in proton exchange membranes for low- and high-temperature fuel cell applications: A review,” *Int J Hydrogen Energy*, vol. 44, no. 12, pp. 6116–6135, Mar. 2019, doi: 10.1016/J.IJHYDENE.2019.01.084.

[15] D. W. Shin, M. D. Guiver, and Y. M. Lee, “Hydrocarbon-Based Polymer Electrolyte Membranes: Importance of Morphology on Ion Transport and Membrane Stability,” *Chemical Reviews*, vol. 117, no. 6. American Chemical Society, pp. 4759–4805, Mar. 22, 2017. doi: 10.1021/acs.chemrev.6b00586.

[16] M. Xu, H. Xue, Q. Wang, and L. Jia, “Sulfonated poly(arylene ether)s based proton exchange membranes for fuel cells,” *Int J Hydrogen Energy*, vol. 46, no. 62, pp. 31727–31753, Sep. 2021, doi: 10.1016/J.IJHYDENE.2021.07.038.

[17] Y. Cheng *et al.*, “High CO tolerance of new SiO2 doped phosphoric acid/polybenzimidazole polymer electrolyte membrane fuel cells at high temperatures of 200–250 °C,” *Int J Hydrogen Energy*, vol. 43, no. 49, pp. 22487–22499, Dec. 2018, doi: 10.1016/J.IJHYDENE.2018.10.036.

[18] J. Zhang *et al.*, “High temperature PEM fuel cells,” *Journal of Power Sources*, vol. 160, no. 2 SPEC. ISS. Elsevier, pp. 872–891, Oct. 06, 2006. doi: 10.1016/j.jpowsour.2006.05.034.

[19] S. Shanmugam, B. Viswanathan, and T. K. Varadarajan, “Synthesis and characterization of silicotungstic acid based organic-inorganic nanocomposite membrane,” *J Memb Sci*, vol. 275, no. 1–2, pp. 105–109, Apr. 2006, doi: 10.1016/j.memsci.2005.09.009.

[20] P. Ahmadi, S. H. Torabi, H. Afsaneh, Y. Sadegheih, H. Ganjehsarabi, and M. Ashjaee, “The effects of driving patterns and PEM fuel cell degradation on the lifecycle assessment of hydrogen fuel cell vehicles,” *Int J Hydrogen Energy*, vol. 45, no. 5, pp. 3595–3608, Jan. 2020, doi: 10.1016/J.IJHYDENE.2019.01.165.

[21] S. M. Javaid Zaidi and T. Matsuura, *Polymer membranes for fuel cells*. Springer US, 2009. doi: 10.1007/978-0-387-73532-0.

[22] M. Rivarolo, D. Rattazzi, T. Lamberti, and L. Magistri, “Clean energy production by PEM fuel cells on tourist ships: A time-dependent analysis,” *Int J Hydrogen Energy*, vol. 45, no. 47, pp. 25747–25757, Sep. 2020, doi: 10.1016/J.IJHYDENE.2019.12.086.

[23] R. Martis, A. Al-Othman, M. Alkasrawi, and M. Tawalbeh, “Fuel cells for carbon capture and power generation: Simulation studies,” *Int J Hydrogen Energy*, vol. 46, no. 8, pp. 6139–6149, Jan. 2021, doi: 10.1016/J.IJHYDENE.2020.10.208.

[24] T. Wilberforce and A. G. Olabi, “Proton exchange membrane fuel cell performance prediction using artificial neural network,” *Int J Hydrogen Energy*, vol. 46, no. 8, pp. 6037–6050, Jan. 2021, doi: 10.1016/J.IJHYDENE.2020.07.263.

[25] C. Song, “Fuel processing for low-temperature and high-temperature fuel cells: Challenges, and opportunities for sustainable development in the 21st century,” *Catal Today*, vol. 77, no. 1–2, pp. 17–49, Dec. 2002, doi: 10.1016/S0920-5861(02)00231-6.

[26] V. Mehta and J. S. Cooper, “Review and analysis of PEM fuel cell design and manufacturing,” *J Power Sources*, vol. 114, no. 1, pp. 32–53, Feb. 2003, doi: 10.1016/S0378-7753(02)00542-6.

[27] M. Shao, “Palladium-based electrocatalysts for hydrogen oxidation and oxygen reduction reactions,” *J Power Sources*, vol. 196, no. 5, pp. 2433–2444, Mar. 2011, doi: 10.1016/J.JPOWSOUR.2010.10.093.

[28] Y. Song, J. M. Fenton, H. R. Kunz, L. J. Bonville, and M. v. Williams, “High-Performance PEMFCs at Elevated Temperatures Using Nafion 112 Membranes,” *J Electrochem Soc*, vol. 152, no. 3, p. A539, 2005, doi: 10.1149/1.1855871.

[29] W. Nsour, T. Taa’mneh, O. Ayadi, and J. al Asfar, “Design of stand-alone proton exchange membrane fuel cell hybrid system under Amman climate,” *Journal of Ecological Engineering*, vol. 20, no. 9, pp. 1–10, 2019, doi: 10.12911/22998993/111800.

[30] S. Mekhilef, R. Saidur, and A. Safari, “Comparative study of different fuel cell technologies,” *Renewable and Sustainable Energy Reviews*, vol. 16, no. 1, pp. 981–989, Jan. 2012, doi: 10.1016/J.RSER.2011.09.020.

[31] T. A. Napp, A. Gambhir, T. P. Hills, N. Florin, and P. S. Fennell, “A review of the technologies, economics and policy instruments for decarbonising energy-intensive manufacturing industries,” *Renewable and Sustainable Energy Reviews*, vol. 30. pp. 616–640, Feb. 2014. doi: 10.1016/j.rser.2013.10.036.

[32] M. Ball and M. Weeda, “The hydrogen economy—Vision or reality?,” *Compendium of Hydrogen Energy*, pp. 237–266, Jan. 2016, doi: 10.1016/B978-1-78242-364-5.00011-7.

[33] T. Hübert, L. Boon-Brett, G. Black, and U. Banach, “Hydrogen sensors – A review,” *Sens Actuators B Chem*, vol. 157, no. 2, pp. 329–352, Oct. 2011, doi: 10.1016/J.SNB.2011.04.070.

[34] M. Kumar Singla, P. Nijhawan, and A. Singh Oberoi, “Hydrogen fuel and fuel cell technology for cleaner future: a review”, doi: 10.1007/s11356-020-12231-8/Published.

[35] M. Ni, M. K. H. Leung, K. Sumathy, and D. Y. C. Leung, “Potential of renewable hydrogen production for energy supply in Hong Kong,” *Int J Hydrogen Energy*, vol. 31, no. 10, pp. 1401–1412, Aug. 2006, doi: 10.1016/J.IJHYDENE.2005.11.005.

[36] R. K. Ahluwalia, X. Wang, and A. Rousseau, “Fuel economy of hybrid fuel-cell vehicles,” *J Power Sources*, vol. 152, no. 1–2, pp. 233–244, Dec. 2005, doi: 10.1016/J.JPOWSOUR.2005.01.052.

[37] V. P. Utgikar and T. Thiesen, “Safety of compressed hydrogen fuel tanks: Leakage from stationary vehicles,” *Technol Soc*, vol. 27, no. 3, pp. 315–320, Aug. 2005, doi: 10.1016/J.TECHSOC.2005.04.005.

[38] C. Huang, W. Yao, A. T-Raissi, and N. Muradov, “Development of efficient photoreactors for solar hydrogen production,” *Solar Energy*, vol. 85, no. 1, pp. 19–27, Jan. 2011, doi: 10.1016/J.SOLENER.2010.11.004.

[39] E. Dündar-Tekkaya and Y. Yürüm, “Mesoporous MCM-41 material for hydrogen storage: A short review,” *Int J Hydrogen Energy*, vol. 41, no. 23, pp. 9789–9795, Jun. 2016, doi: 10.1016/J.IJHYDENE.2016.03.050.

[40] J. M. Ogden, “PROSPECTS FOR BUILDING A HYDROGEN ENERGY INFRASTRUCTURE,” 1999. [Online]. Available: www.annualreviews.org

[41] A. Bakenne, W. Nuttall, and N. Kazantzis, “Sankey-Diagram-based insights into the hydrogen economy of today,” *Int J Hydrogen Energy*, vol. 41, no. 19, pp. 7744–7753, May 2016, doi: 10.1016/J.IJHYDENE.2015.12.216.

[42] M. Kumar Singla, P. Nijhawan, and A. Singh Oberoi, “Hydrogen fuel and fuel cell technology for cleaner future: a review”, doi: 10.1007/s11356-020-12231-8/Published.

[43] C. Yin *et al.*, “Thermal annealing on free volumes, crystallinity and proton conductivity of Nafion membranes,” *Journal of Physics and Chemistry of Solids*, vol. 120, pp. 71–78, Sep. 2018, doi: 10.1016/J.JPCS.2018.04.028.

[44] M. E. Zeynali, F. Mohammadi, and A. Rabiee, “Structural analysis and defect evaluation of ion exchange composite membranes used in electrolysis of sodium

chloride in chlor-alkali process," *Iranian Polymer Journal (English Edition)*, vol. 24, no. 2, pp. 85–93, Feb. 2015, doi: 10.1007/s13726-014-0302-3.

[45] Y. Shi, Z. Lu, L. Guo, and C. Yan, "Fabrication of membrane electrode assemblies by direct spray catalyst on water swollen Nafion membrane for PEM water electrolysis," *Int J Hydrogen Energy*, vol. 42, no. 42, pp. 26183–26191, Oct. 2017, doi: 10.1016/J.IJHYDENE.2017.08.205.

[46] D. J. Kim, M. J. Jo, and S. Y. Nam, "A review of polymer–nanocomposite electrolyte membranes for fuel cell application," *Journal of Industrial and Engineering Chemistry*, vol. 21, pp. 36–52, Jan. 2015, doi: 10.1016/J.JIEC.2014.04.030.

[47] S. Gottesfeld and J. Pafford, "A New Approach to the Problem of Carbon Monoxide Poisoning in Fuel Cells Operating at Low Temperatures," *J Electrochem Soc*, vol. 135, no. 10, pp. 2651–2652, 1988, doi: 10.1149/1.2095401.

[48] M. S. Wilson, J. A. Valerio, and S. Gottesfeld, "Low platinum loading electrodes for polymer electrolyte fuel cells fabricated using thermoplastic ionomers," *Electrochim Acta*, vol. 40, no. 3, pp. 355–363, 1995, doi: 10.1016/0013-4686(94)00272-3.

[49] C. Y. Wong, W. Y. Wong, K. S. Loh, and A. B. Mohamad, "Study of the plasticising effect on polymer and its development in fuel cell application," *Renewable and Sustainable Energy Reviews*, vol. 79, pp. 794–805, Nov. 2017, doi: 10.1016/J.RSER.2017.05.154.

[50] M. Murthy, M. Esayian, A. Hobson, S. Mackenzie, W. Lee, and J. W. van Zee, "Performance of a Polymer Electrolyte Membrane Fuel Cell Exposed to Transient CO Concentrations," 2001, doi: 10.1149/1.1402119.

[51] C. Yang, P. Costamagna, S. Srinivasan, J. Benziger, and A. B. Bocarsly, "Approaches and technical challenges to high temperature operation of proton exchange membrane fuel cells," *J Power Sources*, vol. 103, no. 1, pp. 1–9, Dec. 2001, doi: 10.1016/S0378-7753(01)00812-6.

[52] B. N. Grgur, N. M. Markovic, and P. N. Ross, “Electro-oxidation of H2 and H2 / CO mixtures on carbon-supported PtxMoy alloy catalysts The Electro-oxidation of H 2 and H 2 / CO Mixtures on Carbon-Supported Pt x Mo y Alloy Catalysts,” no. May, 1999, doi: 10.1149/1.1391815.

[53] K. Ketpang, B. Son, D. Lee, and S. Shanmugam, “Porous zirconium oxide nanotube modified Nafion composite membrane for polymer electrolyte membrane fuel cells operated under dry conditions,” *J Memb Sci*, vol. 488, pp. 154–165, Aug. 2015, doi: 10.1016/J.MEMSCI.2015.03.096.

[54] K. T. Adjemian, S. J. Lee, S. Srinivasan, J. Benziger, and A. B. Bocarsly, “Silicon Oxide Nafion Composite Membranes for Proton-Exchange Membrane Fuel Cell Operation at 80-140°C,” *J Electrochem Soc*, vol. 149, no. 3, p. A256, 2002, doi: 10.1149/1.1445431.

[55] B. Son, K. Oh, S. Park, T. G. Lee, D. H. Lee, and O. Kwon, “Study of morphological characteristics on hydrophilicity-enhanced SiO2/Nafion composite membranes by using multimode atomic force microscopy,” *Int J Energy Res*, vol. 43, no. 9, pp. 4157–4169, Jul. 2019, doi: 10.1002/er.4528.

[56] H. Mohammed, A. Al-Othman, P. Nancarrow, M. Tawalbeh, and M. el Haj Assad, “Direct hydrocarbon fuel cells: A promising technology for improving energy efficiency,” *Energy*, vol. 172, pp. 207–219, Apr. 2019, doi: 10.1016/J.ENERGY.2019.01.105.

[57] Y. Zhu, T. Robinson, A. Al-Othman, A. Y. Tremblay, and M. Ternan, “n-Hexadecane Fuel for a Phosphoric Acid Direct Hydrocarbon Fuel Cell,” 2015, doi: 10.1155/2015/748679.

[58] H. Xu, Y. Song, H. R. Kunz, and J. M. Fenton, “Effect of Elevated Temperature and Reduced Relative Humidity on ORR Kinetics for PEM Fuel Cells,” *J Electrochem Soc*, vol. 152, no. 9, p. A1828, 2005, doi: 10.1149/1.1984351.

[59] C. G. Lee, “Effect of temperature on the cathodic overpotential in a molten carbonate fuel cell,” *Journal of Electroanalytical Chemistry*, vol. 701, pp. 36–42, 2013, doi: 10.1016/j.jelechem.2013.04.025.

[60] J. Saavedra, T. Whittaker, Z. Chen, C. J. Pursell, R. M. Rioux, and B. D. Chandler, “Controlling activity and selectivity using water in the Au-catalysed preferential oxidation of CO in H2,” *Nat Chem*, vol. 8, no. 6, pp. 584–589, Jun. 2016, doi: 10.1038/nchem.2494.

[61] X. Gang, L. Qingfeng, H. Aage Hjuler, and N. J. Bjerrum, “Hydrogen Oxidation on Gas Diffusion Electrodes for Phosphoric Acid Fuel Cells in the Presence of Carbon Monoxide and Oxygen,” Electrochemical Society, 1995.

[62] B. Hoyos, N. Munera, and F. Chejne, “CO TOLERANCE IN FUEL CELLS,” *Año*, vol. 75, pp. 123–136, 2008.

[63] A. Chandan *et al.*, “High temperature (HT) polymer electrolyte membrane fuel cells (PEMFC) e A review,” *J Power Sources*, vol. 231, pp. 264–278, 2013, doi: 10.1016/j.jpowsour.2012.11.126.

[64] Y. Cheng *et al.*, “High CO tolerance of new SiO2 doped phosphoric acid/polybenzimidazole polymer electrolyte membrane fuel cells at high temperatures of 200–250 °C,” *Int J Hydrogen Energy*, vol. 43, no. 49, pp. 22487–22499, Dec. 2018, doi: 10.1016/J.IJHYDENE.2018.10.036.

[65] G. S. Ren X, “Electro-osmotic drag of water in poly(perfluorosulfonic acid) membranes,” *The electrochemical society*, vol. 148,Han 2001.

[66] A. Baroutaji *et al.*, “Advancements and prospects of thermal management and waste heat recovery of PEMFC,” *International Journal of Thermofluids*, vol. 9, p. 100064, Feb. 2021, doi: 10.1016/J.IJFT.2021.100064.

[67] J.] Z. Ogumi, Z. Takehara, S. Yoshizawa, “No Title,” *Power Sources*, vol. 131, p. 769, 1984.

[68] R. E. Rosli *et al.*, “A review of high-temperature proton exchange membrane fuel cell (HT-PEMFC) system,” 2016, doi: 10.1016/j.ijhydene.2016.06.211.

[69] W. Nimir *et al.*, “Approaches towards the development of heteropolyacid-based high temperature membranes for PEM fuel cells,” *Int J Hydrogen Energy*, 2021, doi: 10.1016/j.ijhydene.2021.11.174.

[70] J. L. Lu, Q. H. Fang, S. L. Li, and S. P. Jiang, “A novel phosphotungstic acid impregnated meso-Nafion multilayer membrane for proton exchange membrane fuel cells,” *J Memb Sci*, vol. 427, pp. 101–107, Jan. 2013, doi: 10.1016/J.MEMSCI.2012.09.041.

[71] G. Xu, Z. Wei, S. Li, J. Li, Z. Yang, and S. A. Grigoriev, “In-situ sulfonation of targeted silica-filled Nafion for high-temperature PEM fuel cell application,” *Int J Hydrogen Energy*, vol. 44, no. 56, pp. 29711–29716, Nov. 2019, doi: 10.1016/J.IJHYDENE.2019.02.037.

[72] P. Sun, Z. Li, M. Song, S. Wang, X. Yin, and Y. Wang, “Preparation and characterization of zirconium phytate as a novel solid intermediate temperature proton conductor,” *Mater Lett*, vol. 191, pp. 161–164, Mar. 2017, doi: 10.1016/j.matlet.2016.12.076.

[73] M. Kourasi, R. G. A. Wills, A. A. Shah, and F. C. Walsh, “Heteropolyacids for fuel cell applications,” *Electrochim Acta*, vol. 127, pp. 454–466, 2014, doi: 10.1016/j.electacta.2014.02.006.

[74] I. K. Song and M. A. Barteau, “Redox properties of Keggin-type heteropolyacid (HPA) catalysts: effect of counter-cation, heteroatom, and polyatom substitution,” *J Mol Catal A Chem*, vol. 212, no. 1–2, pp. 229–236, Apr. 2004, doi: 10.1016/J.MOLCATA.2003.10.040.

[75] C. Lee *et al.*, “Poly(ether imide) nanofibrous web composite membrane with SiO2/heteropolyacid ionomer for durable and high-temperature polymer electrolyte membrane (PEM) fuel cells,” *Journal of Industrial and Engineering Chemistry*, vol. 74, pp. 7–13, Jun. 2019, doi: 10.1016/J.JIEC.2019.01.034.

[76] V. T. Nguyen *et al.*, “12-Silicotungstic Acid Doped Phosphoric Acid Imbibed Polybenzimidazole for Enhanced Protonic Conductivity for High Temperature Fuel Cell Applications,” *J Electrochem Soc*, vol. 164, no. 6, pp. F504–F513, 2017, doi: 10.1149/2.0331706jes.

[77] C. Lin, T. Haolin, and P. Mu, “Periodic Nafion-silica-heteropolyacids electrolyte t for PEM fuel cell operated near 200°C,” *Int J Hydrogen Energy*, vol. 37, no. 5, pp. 4694–4698, 2012, doi: 10.1016/j.ijhydene.2011.04.116.

[78] C. Lee *et al.*, “Journal of Industrial and Engineering Chemistry Poly (ether imide) nano fi brous web composite membrane with SiO 2 / heteropolyacid ionomer for durable and high-temperature polymer electrolyte membrane (PEM) fuel cells,” *Journal of Industrial and Engineering Chemistry*, vol. 74, pp. 7–13, 2019, doi: 10.1016/j.jiec.2019.01.034.

[79] V. T. Nguyen *et al.*, “12-Silicotungstic Acid Doped Phosphoric Acid Imbibed Polybenzimidazole for Enhanced Protonic Conductivity for High Temperature Fuel Cell Applications,” *J Electrochem Soc*, vol. 164, no. 6, pp. F504–F513, 2017, doi: 10.1149/2.0331706jes.

[80] J. W. Lee *et al.*, “Fabrication of composite membrane based on silicotungstic heteropolyacid doped polybenzimidazole for high temperature PEMFC,” *Int J Electrochem Sci*, vol. 7, no. 7, pp. 6276–6288, 2012.

[81] P. Staiti, M. Minutoli, and S. Hocevar, “Membranes based on phosphotungstic acid and polybenzimidazole for fuel cell application,” *J Power Sources*, vol. 90, no. 2, pp. 231–235, 2000, doi: 10.1016/S0378-7753(00)00401-8.

[82] P. Staiti, “Proton conductive membranes based on silicotungstic acid/silica and polybenzimidazole,” *Mater Lett*, vol. 47, no. 4–5, pp. 241–246, 2001, doi: 10.1016/S0167-577X(00)00241-X.

[83] P. Staiti and M. Minutoli, “In ¯ uence of composition and acid treatment on proton conduction of composite polybenzimidazole membranes,” vol. 94, pp. 9–13, 2001.

[84] R. He, Q. Li, G. Xiao, and N. J. Bjerrum, “Proton conductivity of phosphoric acid doped polybenzimidazole and its composites with inorganic proton conductors,” *J Memb Sci*, vol. 226, no. 1–2, pp. 169–184, 2003, doi: 10.1016/j.memsci.2003.09.002.

[85] V. Ramani, H. R. Kunz, and J. M. Fenton, “Stabilized heteropolyacid/Nafion® composite membranes for elevated temperature/low relative humidity PEFC operation,” *Electrochim Acta*, vol. 50, no. 5, pp. 1181–1187, 2005, doi: 10.1016/j.electacta.2004.08.015.

[86] H. J. Kim, Y. G. Shul, and H. Han, “Sulfonic-functionalized heteropolyacid-silica nanoparticles for high temperature operation of a direct methanol fuel cell,” *J Power Sources*, vol. 158, no. 1, pp. 137–142, 2006, doi: 10.1016/j.jpowsour.2005.10.001.

[87] J. Zhang, S. Chen, H. Bai, S. Lu, Y. Xiang, and S. P. Jiang, “Effects of phosphotungstic acid on performance of phosphoric acid doped polyethersulfone-polyvinylpyrrolidone membranes for high temperature fuel cells,” *Int J Hydrogen Energy*, vol. 46, no. 19, pp. 11104–11114, Mar. 2021, doi: 10.1016/J.IJHYDENE.2020.07.082.

[88] L. Bai *et al.*, “Fabrication of phosphotungstic acid functionalized mesoporous silica composite membrane by alternative tape-casting incorporating phase inversion technique,” *J Power Sources*, vol. 246, pp. 522–530, 2014, doi: 10.1016/j.jpowsour.2013.07.119.

[89] J. Zeng and S. P. Jiang, “Characterization of high-temperature proton-exchange membranes based on phosphotungstic acid functionalized mesoporous silica nanocomposites for fuel cells,” *Journal of Physical Chemistry C*, vol. 115, no. 23, pp. 11854–11863, 2011, doi: 10.1021/jp201250r.

[90] F. Meng *et al.*, “Structural and transport effects of doping perfluorosulfonic acid polymers with the heteropoly acids, H3PW12O40 or H4SiW12O40,” *Electrochim Acta*, vol. 53, no. 3, pp. 1372–1378, Dec. 2007, doi: 10.1016/J.ELECTACTA.2007.06.047.

[91] M. Aparicio, J. Mosa, M. Etienne, and A. Durán, “Proton-conducting methacrylate-silica sol-gel membranes containing tungstophosphoric acid,” *J Power Sources*, vol. 145, no. 2, pp. 231–236, 2005, doi: 10.1016/j.jpowsour.2005.01.071.

[92] S. M. J. Zaidi, S. D. Mikhailenko, G. P. Robertson, M. D. Guiver, and S. Kaliaguine, “Proton conducting composite membranes from polyether ether ketone and heteropolyacids for fuel cell applications,” *J Memb Sci*, vol. 173, no. 1, pp. 17–34, Jul. 2000, doi: 10.1016/S0376-7388(00)00345-8.

[93] Y. S. Kim, F. Wang, M. Hickner, T. A. Zawodzinski, and J. E. McGrath, “Fabrication and characterization of heteropolyacid (H3PW12O40)/directly polymerized sulfonated poly(arylene ether sulfone) copolymer composite membranes for higher temperature fuel cell applications,” *J Memb Sci*, vol. 212, no. 1–2, pp. 263–282, 2003, doi: 10.1016/S0376-7388(02)00507-0.

[94] T. F. Cells, “A Composite Membrane of Caesium Salt of Heteropolyacids/Quaternary Diazabicyclo-Octane Polysulfone with Poly (Tetrafluoroethylene) for Intermediate Temperature Fuel Cells,” pp. 384–394, 2012, doi: 10.3390/membranes2030384.

[95] Y. S. Ye, J. Rick, and B. J. Hwang, “Water soluble polymers as proton exchange membranes for fuel cells,” *Polymers*, vol. 4, no. 2. pp. 913–963, 2012. doi: 10.3390/polym4020913.

[96] S. Lee, W. Jang, S. Choi, K. Tharanikkarasu, Y. Shul, and H. Han, “Suif onated polyimide and poly (ethylene glycol) diacrylate based semi-interpenetrating polymer network membranes for fuel cells,” *J Appl Polym Sci*, vol. 104, no. 5, pp. 2965–2972, Jun. 2007, doi: 10.1002/app.25966.

[97] H. Y. Chang, R. Thangamuthu, and C. W. Lin, “Structure–property relationships in PEG/SiO2 based proton conducting hybrid membranes—A 29Si CP/MAS solid-state NMR study,” *J Memb Sci*, vol. 228, no. 2, pp. 217–226, Jan. 2004, doi: 10.1016/J.MEMSCI.2003.10.010.

[98] H. Jodat, M. Mortezaei, H. Mahdavi, L. Ahmadian-Alam, and P. Manafi, “Effect of polyethylene glycol on sulfonated polyether imide (SPEI) for fuel cell applications,” *Polymer Science - Series B*, vol. 58, no. 2, pp. 205–213, Mar. 2016, doi: 10.1134/S1560090416020020.

[99] R. P. Pugalenthi, G. Cao, and R. P. Manimuthu, “Cross-linked SPEEK-PEG-APTEOS-modified CaTiO3perovskites for efficient acid-base cation-exchange membrane fuel cell,” *Energy and Fuels*, vol. 34, no. 8, pp. 10087–10099, Aug. 2020, doi: 10.1021/acs.energyfuels.0c01933.

[100] Q. L. Chen, K. J. Wu, and C. H. He, “Thermal conductivity of ionic liquids at atmospheric pressure: Database, analysis, and prediction using a topological

index method," *Ind Eng Chem Res*, vol. 53, no. 17, pp. 7224–7232, Apr. 2014, doi: 10.1021/ie403500w.

[101] M. Díaz, A. Ortiz, and I. Ortiz, "Progress in the use of ionic liquids as electrolyte membranes in fuel cells," *J Memb Sci*, vol. 469, pp. 379–396, Nov. 2014, doi: 10.1016/J.MEMSCI.2014.06.033.

[102] J. Yang, Y. Wang, G. Yang, and S. Zhan, "New anhydrous proton exchange membranes based on fluoropolymers blend imidazolium poly (aromatic ether ketone)s for high temperature polymer electrolyte fuel cells," *Int J Hydrogen Energy*, vol. 43, no. 17, pp. 8464–8473, Apr. 2018, doi: 10.1016/j.ijhydene.2018.03.128.

[103] T. Zhang, G. Yu, X. Liang, N. Zhao, F. Zhang, and F. Qu, "Development of anion conducting zeolitic imidazolate framework bottle around ship incorporated with ionic liquids," *Int J Hydrogen Energy*, vol. 44, no. 29, pp. 14481–14492, Jun. 2019, doi: 10.1016/J.IJHYDENE.2019.04.044.

[104] J. Fang, M. Lyu, X. Wang, Y. Wu, and J. Zhao, "Synthesis and performance of novel anion exchange membranes based on imidazolium ionic liquids for alkaline fuel cell applications," *J Power Sources*, vol. 284, pp. 517–523, Jun. 2015, doi: 10.1016/J.JPOWSOUR.2015.03.065.

[105] H. Ye, J. Huang, J. J. Xu, N. K. A. C. Kodiweera, J. R. P. Jayakody, and S. G. Greenbaum, "New membranes based on ionic liquids for PEM fuel cells at elevated temperatures," *J Power Sources*, vol. 178, no. 2, pp. 651–660, Apr. 2008, doi: 10.1016/J.JPOWSOUR.2007.07.074.

[106] C. J. Lawrence, "The mechanics of spin coating of polymer films," *Physics of Fluids*, vol. 31, no. 10, pp. 2786–2795, Oct. 1988, doi: 10.1063/1.866986.

[107] F. Tasselli, "Membrane Preparation Techniques," in *Encyclopedia of Membranes*, Springer Berlin Heidelberg, 2014, pp. 1–3. doi: 10.1007/978-3-642-40872-4_1825-1.

[108] A. Al-Othman, A. Y. Tremblay, W. Pell, Y. Liu, B. A. Peppley, and M. Ternan, "The effect of glycerol on the conductivity of Nafion-free ZrP/PTFE composite

membrane electrolytes for direct hydrocarbon fuel cells," *J Power Sources*, vol. 199, pp. 14–21, Feb. 2012, doi: 10.1016/J.JPOWSOUR.2011.09.104.

[109] "Silicotungstic acid," *Wikipedia*. 2022. Accessed: Nov. 11, 2022. [Online]. Available: https://en.wikipedia.org/wiki/Silicotungstic_acid

[110] "silicotungstic acid hydrate," *ChemSrc*, Nov. 01, 2022. [online]. https://www.chemsrc.com/en/cas/12027-43-9_914747.html (accessed Nov. 11, 2022).

[111] C. W. Lin, R. Thangamuthu, and P. H. Chang, "PWA-doped PEG/SiO2 proton-conducting hybrid membranes for fuel cell applications," *J Memb Sci*, vol. 254, no. 1–2, pp. 197–205, Jun. 2005, doi: 10.1016/J.MEMSCI.2005.01.007.

[112] H. Y. Lee, S. K. Kim, M. R. Lee, D. H. Peck, Y. C. Kang, and C. S. Kim, "Reduced mass transport resistance in polymer electrolyte membrane fuel cell by polyethylene glycol addition to catalyst ink," *Int J Hydrogen Energy*, vol. 44, no. 1, pp. 354–361, Jan. 2019, doi: 10.1016/J.IJHYDENE.2018.08.134.

[113] A. Alashkar, A. Al-Othman, M. Tawalbeh, and M. Qasim, "A Critical Review on the Use of Ionic Liquids in Proton Exchange Membrane Fuel Cells," *Membranes*, vol. 12, no. 2. MDPI, Feb. 01, 2022. doi: 10.3390/membranes12020178.

[114] A. Ka'ki, A. Alraeesi, A. Al-Othman, and M. Tawalbeh, "Proton conduction of novel calcium phosphate nanocomposite membranes for high temperature PEM fuel cells applications," *Int J Hydrogen Energy*, vol. 46, no. 59, pp. 30641–30657, Aug. 2021, doi: 10.1016/J.IJHYDENE.2021.01.013.

[115] M. Tawalbeh, A. Al-Othman, A. Ka'ki, A. Farooq, and M. Alkasrawi, "Lignin/zirconium phosphate/ionic liquids-based proton conducting membranes for high-temperature PEM fuel cells applications," *Energy*, vol. 260, Dec. 2022, doi: 10.1016/j.energy.2022.125237.

[116] D. G. Kuroda, P. K. Singh, and R. M. Hochstrasser, "Differential hydration of tricyanomethanide observed by time resolved vibrational spectroscopy," *Journal of Physical Chemistry B*, vol. 117, no. 16, pp. 4354–4364, Apr. 2013, doi: 10.1021/jp3069333.

[117] C. M. S. S. Neves *et al.*, "Systematic study of the thermophysical properties of imidazolium-based ionic liquids with cyano-functionalized anions," *Journal of Physical Chemistry B*, vol. 117, no. 35, pp. 10271–10283, Sep. 2013, doi: 10.1021/jp405913b.

[118] E. Fontananova, F. Trotta, J. C. Jansen, and E. Drioli, "Preparation and characterization of new non-fluorinated polymeric and composite membranes for PEMFCs," *J Memb Sci*, vol. 348, no. 1–2, pp. 326–336, Feb. 2010, doi: 10.1016/J.MEMSCI.2009.11.020.

[119] L. F. Tóth, P. de Baets, and G. Szebényi, "Processing analysis of nanoparticle filled PTFE: Restrictions and limitations of high temperature production," *Polymers (Basel)*, vol. 12, no. 9, Sep. 2020, doi: 10.3390/POLYM12092044.

[120] Z. Li *et al.*, "Enhanced proton conductivity of nafion hybrid membrane under different humidities by incorporating metal-organic frameworks with high phytic acid loading," *ACS Appl Mater Interfaces*, vol. 6, no. 12, pp. 9799–9807, Jun. 2014, doi: 10.1021/am502236v.

[121] A. Barylski *et al.*, "Novel organic material induced by electron beam irradiation for medical application," *Polymers (Basel)*, vol. 12, no. 2, Feb. 2020, doi: 10.3390/polym12020306.

[122] P. Wang, C. Li, H. Gong, X. Jiang, H. Wang, and K. Li, "Effects of synthesis conditions on the morphology of hydroxyapatite nanoparticles produced by wet chemical process," *Powder Technol*, vol. 203, no. 2, pp. 315–321, Nov. 2010, doi: 10.1016/J.POWTEC.2010.05.023.

[123] B. Kwakye-Awuah, E. Von-Kiti, I. Nkrumah, R. Erdoo Ikyreve, I. Radecka, and C. Williams, "Parametric, equilibrium, and kinetic study of the removal of salt ions from Ghanaian seawater by adsorption onto zeolite X," *Desalination Water Treat*, vol. 57, no. 45, pp. 21654–21663, Sep. 2016, doi: 10.1080/19443994.2015.1128361.

[124] X. Rong, F. Qiu, C. Zhang, L. Fu, Y. Wang, and D. Yang, "Preparation, characterization and photocatalytic application of TiO2–graphene photocatalyst

under visible light irradiation," *Ceram Int*, vol. 41, no. 2, pp. 2502–2511, Mar. 2015, doi: 10.1016/J.CERAMINT.2014.10.072.

[125] R. M. Nauman Javed, A. Al-Othman, P. Nancarrow, and M. Tawalbeh, "Zirconium silicate-ionic liquid membranes for high-temperature hydrogen PEM fuel cells," *Int J Hydrogen Energy*, May 2022, doi: 10.1016/J.IJHYDENE.2022.05.009.

[126] S. Vavra, N. Vilà, A. Lotsari, A. Walcarius, and A. Martinelli, "An imidazolium ionic liquid as effective structure-directing agent for the fabrication of silica thin films with vertically aligned nanochannels," *Microporous and Mesoporous Materials*, p. 110407, Jul. 2020, doi: 10.1016/J.MICROMESO.2020.110407.

[127] U. P. Agarwal, S. A. Ralph, C. Baez, R. S. Reiner, and S. P. Verrill, "Effect of sample moisture content on XRD-estimated cellulose crystallinity index and crystallite size," *Cellulose*, vol. 24, no. 5, pp. 1971–1984, May 2017, doi: 10.1007/s10570-017-1259-0.

[128] D. D. Le Pevelen, "Small Molecule X-Ray Crystallography, Theory and Workflow," *Encyclopedia of Spectroscopy and Spectrometry*, pp. 2559–2576, Jan. 2010, doi: 10.1016/B978-0-12-374413-5.00359-6.

Vita

Wessam Ahmed Mohamed Nimir was born in 1995, in Doha, Qatar. She received her primary and secondary education in Khartoum, Sudan. She received her B.Sc. degree in Chemical Engineering from the Khartoum University in 2017, from 2012 to 2017.

In January 2021, she joined the Chemical Engineering master's program in the American University of Sharjah as a graduate research assistant. During her master's study, she co-authored one review paper and two papers which were presented in two conferences. Her research interest is in polymer electrolyte membrane fuel cells.